JOURNAL OF GEOPHYSICAL RESEARCH, VOL. 100, NO. B12, PAGES 24,015–24,036, DECEMBER 10, 1995

Earthquake source scaling relationships from -1 to 5 M_L using seismograms recorded at 2.5-km depth

Rachel E. Abercrombie

Department of Earth Sciences, University of Southern California, Los Angeles

Abstract. The scaling relationships of earthquake sources less than about magnitude 3 have been the subject of considerable controversy over the last two decades. Studies of such events have shown a tendency for the constant stress drop, self similarity of larger earthquakes to breakdown at small magnitudes, and an apparent minimum source dimension of about 100 m has been observed. Other studies showed that this apparent breakdown in scaling could be an artifact of severe near-surface attenuation, limiting the spatial resolution of surface data. In this study, source parameters are determined for over 100 nearby, tectonic earthquakes, from recordings at a depth of 2.5 km (in granite) in the Cajon Pass scientific drill hole, southern California. Comparison of the seismograms recorded at this depth with those at the wellhead clearly demonstrates the effect of the severe attenuation in the upper kilometers of the Earth's crust. Source parameters are calculated by spectral modeling of three-component P and S waves, assuming four source models based on the Brune ω^{-2} ($n = 2$) model. In model 1, $n = 2$ is fixed, and Q of P and S waves is determined to be 912 (581-1433) and 1078 (879-1323), respectively (the numbers in parentheses are ±1 standard deviation). In model 2, $Q_P = Q_S = 1000$ is assumed and n is allowed to vary. The ω^{-2} model is a good average for the data set, but there is some real scatter supported by the data. In model 3, $Q_P = Q_S = 1000$ is also assumed and ω^{-2} is constrained, and in model 4, attenuation is ignored and n is allowed to vary. Source dimensions of less than 10 m are observed for all four models, 10 times smaller than the proposed "minimum". No breakdown in constant stress drop scaling is seen in the downhole data (approximately M_L -1 to 5.5, $M_0 = 10^9$-10^{16} Nm). The ratio between radiated seismic energy (estimated by integrating the velocity squared spectra with adequate signal bandwidth) and seismic moment appears to decrease gradually with decreasing moment in the magnitude range -1 to 7. This is not incompatible with a constant stress drop but could result from errors in calculating energy. The ratio of the S wave energy to that radiated by the P waves is about 14, after correction for attenuation. This low value is consistent with the corner frequency shift of about 1.3. This corner frequency shift is observed for all four source models and therefore is interpreted as being source controlled.

Introduction

One of the fundamental problems facing seismologists is how to distinguish amongst source, path, and site effects in seismograms. This problem is perhaps at its worst in the study of small earthquakes because the higher frequencies needed to define the smaller sources are most affected by attenuation along the path and by near-surface site effects. The source parameters seismic moment and source dimension have been determined for a large number of earthquakes over a wide range of magnitudes (~0 to 7) in the past two decades. Compilations of these results have shown that seismic moment is proportional to the source dimension cubed, corresponding to the stress drop being independent of magnitude. Earthquake stress drops are not well constrained because of their dependence on the cube of the source dimension, but are typically between 0.1 and 100 MPa [e.g., *Hanks*, 1977; *Abercrombie and Leary*, 1993]. This scale invariance of the earthquake rupture process was first suggested by *Aki* [1967] and is consistent with observations that many geological processes are self-similar over a very wide range of scales (see *Turcotte* [1989] for a review). A number of studies of smaller earthquakes, however, have found an apparent breakdown in self-similarity for earthquake sources less than about magnitude 3 [e.g., *Archuleta et al.*, 1982; *Guo et al.*, 1992]. Below this magnitude the earthquakes appear to have a constant dimension (of about 100 m), and stress drop appears to decrease with seismic moment. This breakdown has been interpreted as possibly resulting from geometrical controls on earthquake source dimension, and is similar to the width of major fault zones. The width of the seismogenic crust is known to act as a geometrical constraint on earthquake rupture propagation and results in a change in scaling relationships at very large magnitudes [*Shimazaki*, 1986], and so such an idea is not without precedent. Also, frictional models of the nucleation of seismic slip, based on laboratory experiments find that dynamic instability begins only after a certain minimum slip displacement has taken place [*Dieterich*, 1986]. If a minimum source dimension is found to exist for tectonic earthquakes then it would enable such frictional models to be more closely related to fault zone structure.

Other researchers, however, including *Hanks* [1982], *Anderson and Hough* [1984], and *Anderson* [1986] have argued that this

[1]Now at Institute of Geological and Nuclear Sciences, Wellington, New Zealand.

Paper number 95JB02397.
0148-0227/95/95JB-02397$05.00

apparent minimum earthquake source dimension is entirely unrelated to the earthquake source and is merely an artifact of severe attenuation in the near-surface rocks. *Hanks* [1982] compares the frequency above which acceleration spectra start to fall off (f_{max}) from earthquakes recorded at a number of different sites, and finds some evidence that these high-frequency effects are related to the recording site conditions. *Anderson* [1986] demonstrates that near-surface attenuation could, in theory, remove the high-frequency energy needed to constrain the length of smaller sources from the seismograms, and so cause the apparent breakdown in scaling.

Recent studies of small-earthquake sources have attempted to correct for whole path and local site attenuation using theoretical [e.g. *Boatwright et al.*, 1991] and empirical [e.g., *Frankel and Wennerberg*, 1989] Green's functions, but have been unable to resolve the controversy satisfactorily. The combination of surface noise and high attenuation limits the bandwidth available for analysis and signal frequencies higher than about 50 Hz needed to constrain smaller earthquake sources cannot ordinarily be seen by surface instruments. A more straightforward approach is to record the seismic waves before they travel through the near-surface rocks. Recent recording of local earthquakes in boreholes at depths of 200 to 300 m at Parkfield *[Blakeslee and Malin*, 1991] and Anza [*Aster and Shearer*, 1991] and elsewhere has shown that the background noise level is considerably lower at depth than at the surface, and that attenuation in the upper few hundred meters is very high, with compressional and shear Q values between 5 and 30, independent of rock type. Observation of the earthquake spectra, however, shows that significant attenuation is occurring at greater depths and that the controversies outlined above cannot be clearly resolved with these shallow data.

In this study, source parameters are determined from local earthquakes recorded at a depth of 2.5 km, about 10 times deeper than previous studies, at Cajon Pass in southern California. The results confirm the preliminary analysis of *Abercrombie and Leary* [1993] that there is no breakdown in self similarity of earthquake sources above about -1 M_L. Source dimensions a factor of 10 smaller than the proposed "minimum" value proposed by *Archuleta et al.* [1982] and *Guo et al.* [1992] are observed, and it is clear that the apparent breakdown in self-similarity of earthquake sources at about 3 M_L is simply an artifact of severe attenuation in the upper kilometers of the Earth's crust.

Data

A triaxial set of 10 Hz, high-temperature geophones was installed at a depth of 2.5 km (105°C) in the Cajon Pass scientific drill hole, in southern California, about 4 km from the San Andreas fault (Figure 1). The hole was drilled through 500 m of sediment followed by 200 to 500 m of highly fractured granite, and then into largely uninterrupted crystalline granite [*Silver and James*, 1988]. During the 2 years of geophone operation (August 1991 to August 1993), several thousand tectonic earthquakes in the vicinity of the San Andreas fault were recorded. About 90% of

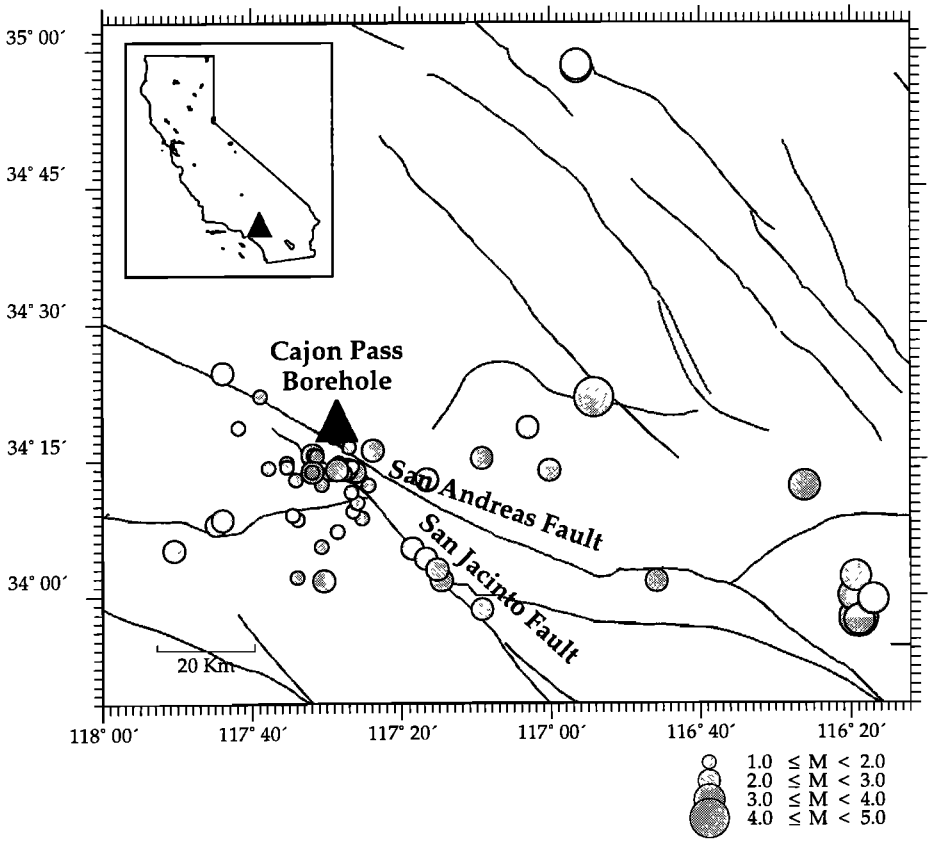

Figure 1. Map showing the Cajon Pass borehole (triangle) and the San Andreas and San Jacinto faults. Also plotted are the epicenters of the earthquakes considered in this study which were large enough to trigger the SCSN. The inset shows the location of the borehole (triangle) in the state of California.

these were too small to trigger the Southern California Seismic Network (SCSN), or to be observed above surface noise by the three-component (L22, 2 Hz) sensor installed at the wellhead [*Abercrombie*, 1995]. Recording was carried out at 500 samples/s downhole, with the exception of 1 month in which the rate was increased to 1000 samples/s. The surface instrument was triggered by the downhole and was recorded at 250 samples/s.

Figure 2 shows a comparison of the downhole and surface recordings of three local earthquakes. The downhole seismograms contain higher frequency energy and less scattered energy than those recorded at the surface. It is clear that a significant amount of both the intrinsic and scattering attenuation affecting surface recorded seismograms occurs in the upper few kilometers. *Abercrombie and Leary* [1993] and R. E. Abercrombie (Near surface attenuation and site effects from comparison of surface and deep borehole recordings, submitted to *Bulletin of the Seimological Society of America*, 1995) compare the downhole and surface spectra for a number of earthquakes, finding that passage of the seismic waves through the near-surface rocks resulted in amplification by a factor of 5 to 10 below about 10 Hz, and severe attenuation of the higher frequencies. They estimate Q to be about 30 for the upper 2.5 km.

In the present study, 115 of the earthquakes recorded downhole with high signal to noise are selected for analysis to determine source parameters and investigate the scaling of small sources with respect to larger ones. They occur at hypocentral distances of 5 to 120 km from the borehole, with 78 of the earthquakes being within 20 km of the borehole. The more distant events are principally aftershocks of the 1992 Joshua Tree and Landers earthquakes (~90 to 120 km) and the 1992 Big Bear event (~50 to 80 km). Sixty-three of these earthquakes were large enough to trigger the SCSN (M_L 1.1 to 4.6).

Spectral Analysis

The simple waveforms of the downhole seismograms render them amenable to standard frequency domain analysis as proposed by *Brune* [1970] and revised by *Madariaga* [1976]. The choice of standard, commonly used techniques to analyze the downhole seismograms facilitates comparison with previous shallow and surface studies. Time windows around both P and S waves individually are selected on all three components. The length of the time windows used is dependent on the earthquake magnitude, as larger events have longer source durations. One-second windows are used for the smallest events ($<M_L$ 3), 2-s windows for events $3 \le M_L < 4$, and 4-s windows for the larger earthquakes. The displacement spectra of both P and S waves on all three components for all events are determined using the multi-tapering technique developed by *Park et al.* [1987]. The instrument response is then removed. At 2.5 km the seismic waves have not been refracted to vertical ray paths, and so P and S energy is observed on all three components, see Figure 2. The P and S spectra of all three components are then all modeled individually in the bandwidth in which the signal is at least 5 times the noise level (0.5-6 to 80-140 Hz)

Equation (1) is the general model used here to fit the displacement spectra of both P and S waves.

$$\Omega(f) = \frac{\Omega_0 e^{-(\pi f t/Q)}}{\left[1+(f/f_c)^{\gamma n}\right]^{1/\gamma}} \quad (1)$$

Where Ω_0 is the long period amplitude, f the frequency, f_C the corner frequency, t the travel time of the wave being considered, Q the frequency independent quality factor, n the high-frequency fall off rate (on a log-log plot), and γ is a constant. Travel time (t) and hypocentral distance (R) are determined from the delay time between the P and S arrivals, assuming a P wave velocity (α) of 6 km/s and S wave velocity (β) of $\alpha/\sqrt{3}$ throughout [*Abercrombie*, this issue]. If $t = 0$, $n = 2$, and $\gamma = 1$, equation 1 is the spectral shape proposed by *Brune* [1970]. *Boatwright* [1980] proposed a modified version of the spectral shape with $\gamma = 2$. This produces a sharper corner than the original Brune model which Boatwright found better matched his data. Initially, the spectra recorded here are fit within the original Brune spectrum ($\gamma = 1$). As can be seen in Figure 3 (a), however, some of the spectra at short hypocentral distances have very sharp corners. The fitting algorithm used was unable to converge for over 30% of the P spectra ($R < 15$ km) using this model, within the chosen termination tolerance of the simplex algorithm (10^{-4}). A Nelder-Meade simplex algorithm (in MATLAB™) is used to determine iteratively the best fitting parameters for all of the models considered here. The revised version of the source model proposed by *Boatwright* [1980] with $\gamma = 2$ is therefore preferred (adequately fitting 95% of the same spectra with lower variances) as a better model of the data in this study.

The high frequency falloff $n = 2$ is regularly assumed as a good average for a set of data following the work of *Brune* [1970] and *Madariaga* [1976]. The spectra are therefore fit initially assuming $n = 2$ and $\gamma = 2$ to find the free parameters Ω_0, f_C, and Q. This first model is termed model 1 and the results (together with those of the later models) are shown in Tables 1, 2, and 3.

The Q values determined using model 1 for P (Q_P) and S (Q_S) waves are plotted in Figure 4 as a function of distance. There is no obvious dependence of either Q_P or Q_S on distance, suggesting that $n = 2$ is a good average value of falloff for these data. The scatter is the greatest in the events with the shortest travel times which have experienced too little attenuation to constrain Q well. Using only the 38 earthquakes with $R \ge 20$ km, the geometrical mean Q values are Q_P = 912 (581-1433) and Q_S = 1078 (879-1323). The numbers in parentheses following the mean values (here and in the rest of the paper) are ±1 standard deviation.

In order to investigate the various model parameters further and their resolution, three more models are fit to the spectra. In the first two, the Q values are constrained from the results of model 1: $Q_P = Q_S = 1000$. In model 2, n is allowed to vary to investigate what sort of variation in falloff is consistent with the data. In model 3, n is constrained to be 2, leaving only Ω_0 and f_C as free parameters to check that they are not being ill determined by too many free parameters in the other models. In model 4, the effect of ignoring Q is investigated with the exponential function in equation (1) set to 1 and Ω_0, f_C , and n varying. This model fits the nearest events relatively well, but more distant events poorly. Examples of the model fits to two events, a small (1.7 M_L)

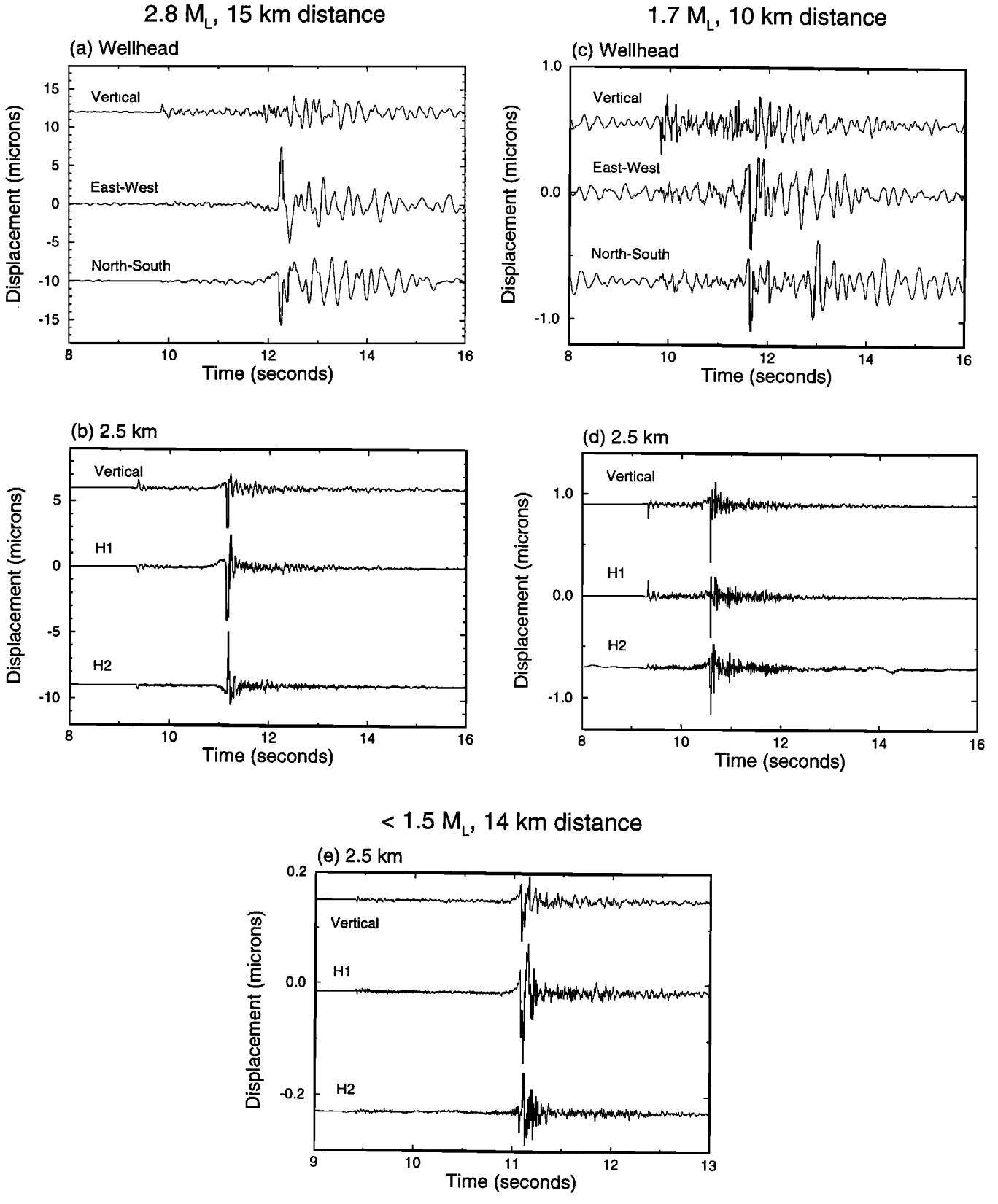

Figure 2. Comparison of earthquake seismograms recorded at the wellhead and at 2.5 km depth. All the seismograms have been corrected for instrument response, and are flat to displacement between 1 and 200 Hz. (a and c) Surface recordings. (b and d) The same two earthquakes recorded at 2.5 km. Notice the low background noise level downhole, also the higher frequency *P* and *S* arrivals and significant reduction in scattered energy (coda) with respect to the surface recordings. (e) Downhole recording of an earthquake too small to trigger the SCSN or be seen above the noise level on the wellhead seismometer.

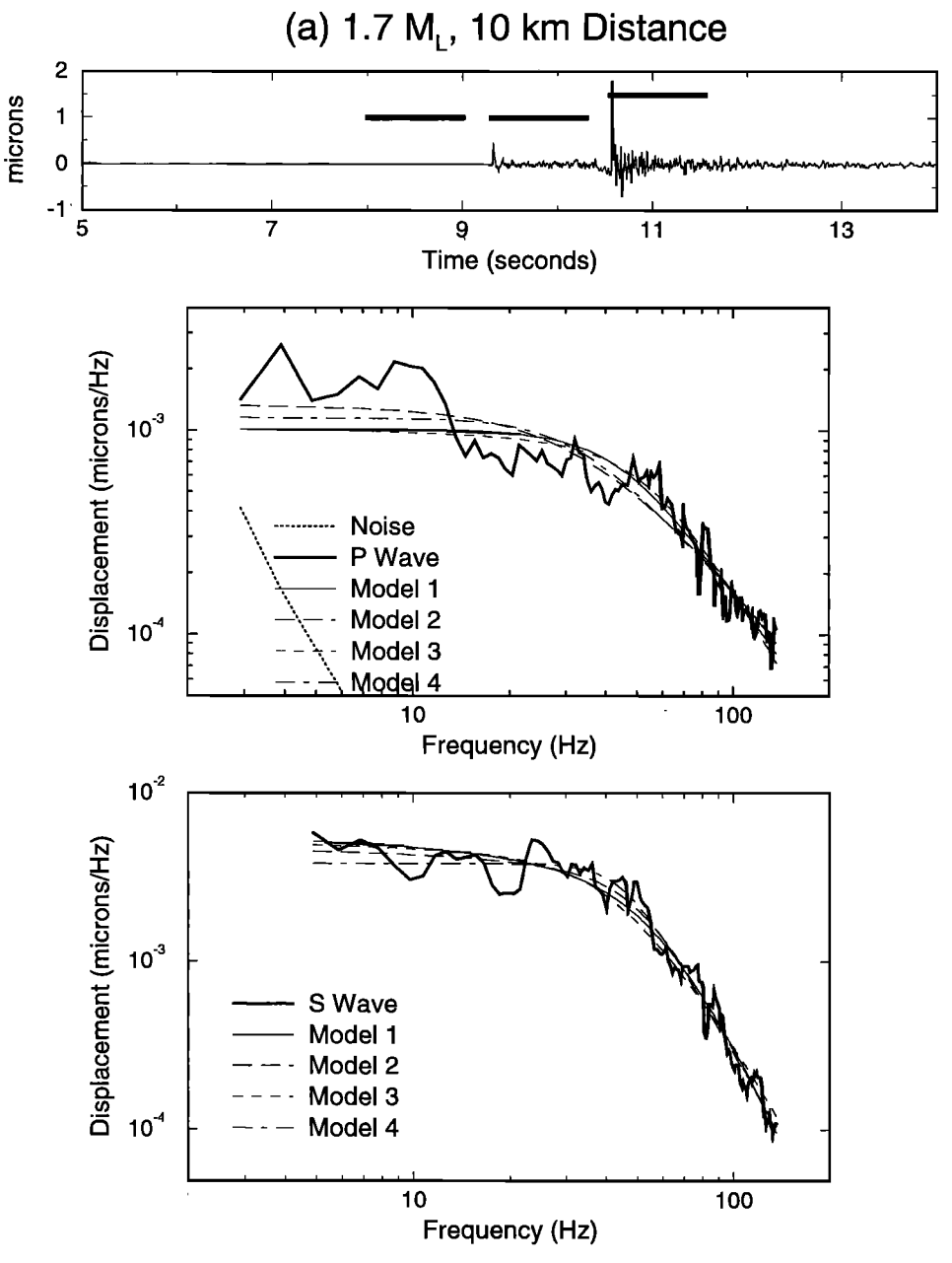

Figure 3. Spectral modeling of P and S waves. The spectra from (a) a local, small earthquake and (b) a larger, more distant earthquake are compared. The solid bars on the seismogram plots (both vertical component) indicate the time windows used to calculate the noise, P, and S spectra respectively. All spectra are calculated from the recorded seismograms and then corrected for the instrument response. The upper spectra are those of the P waves, and the lower plots are those of the S waves. The fits of the four models are shown. There is little difference between them although model 4 (no Q) is a reasonable fit to the event in Figure 3a but not to the more distant event in Figure 3b; compare the relatively linear high-frequency falloff of the nearer event to the more exponential curve of the more distant, event which has experienced considerably more attenuation. Model parameters are given in Table 1.

earthquake, 10 km hypocentral distance from the borehole, and a larger (4.1 M_L) more distant earthquake (53 km), are shown in Figure 3. Clearly there is little to choose between the models. This is borne out by the results in Tables 2 and 3. The variances are similar for all four models as are the various resulting parameters and their ratios.

Figure 5 shows the effect of including $Q_P = Q_S = 1000$ on the high frequency falloff values, n. The increase in n with distance seen in the raw spectra can be attributed to attenuation, but some variation in n seems supported by the data. The results from all four models are very similar but as it would seem more plausible that n should vary over such short distances than Q, the results of model 2 are those preferred in this paper (see also the discussion section).

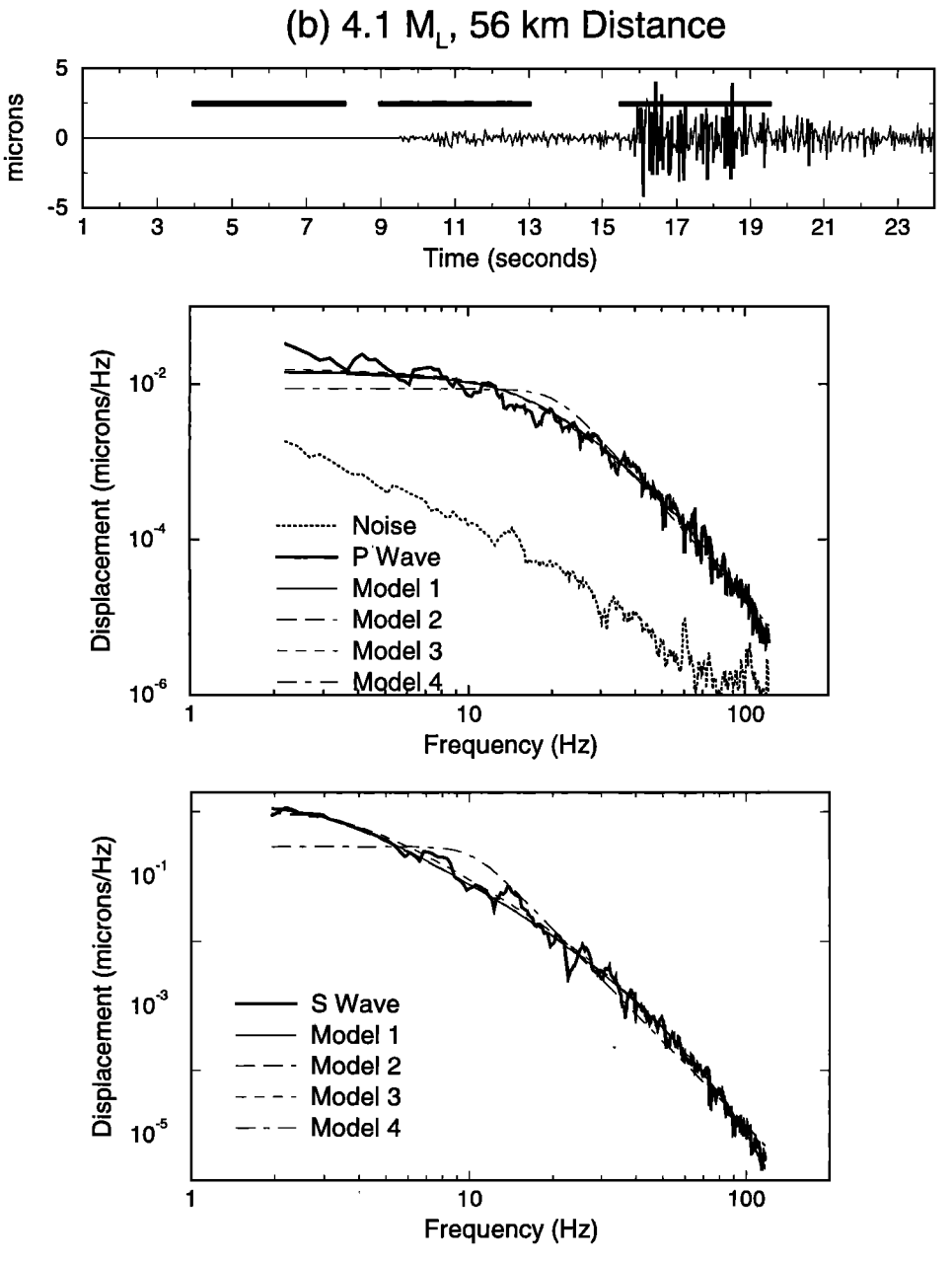

Figure 3. (continued)

Results

Seismic Moment, Source Dimension and Stress Drop

The source parameters seismic moment (M_0), and source radius (r) are calculated from Ω_0 and f_C for all four models using

$$M_0 = \frac{4\pi\rho c^3 R\sqrt{\Omega_0(\mathrm{Z})^2 + \Omega_0(\mathrm{H1})^2 + \Omega_0(\mathrm{H2})^2}}{U_{\phi\theta}} \quad (2)$$

[*Brune*, 1970]

$$r = \frac{3k\beta}{\left(f_c(\mathrm{Z}) + f_c(\mathrm{H1}) + f_c(\mathrm{H2})\right)} \quad (3)$$

[*Madariaga*, 1976].

The density (ρ) is taken to be 2700 kg/m^3, c is the wave velocity (α for P waves and β for S waves), R is the hypocentral distance (in meters, from the S-P time), $U_{\phi\theta}$ is the mean radiation pattern (0.52 and 0.63 for P and S waves, respectively [*Aki and Richards*, 1980]), and k is 0.32 for P waves and 0.21 for S waves [*Madariaga*, 1976]. When Ω_0 estimates could not be reliably made on all three components (Z, H1, and H2), the available components were multiplied by the relevant scaling factor, assuming that the missing values were equal to the mean of the available values. The source dimension is determined from the mean of the available f_C measurements. The dynamic solution of *Madariaga* [1976] for both P and S waves is preferred to the static S wave only model of *Brune* [1970]. A ratio of 1.5 between the P and S corner frequencies is predicted by *Madariaga* [1976]. This

Table 1a. Source Parameter Results From Models 1 and 2

Event	M_L	D, km	Model 1 (n=2, Q=?)						Model 2 (n=?, Q_P=Q_S=1000)					
			M_0P, N m	M_0S, N m	rP, m	rS, m	Q_P	Q_S	M_0P, N m	M_0S, N m	rP, m	rS, m	nP	nS
92098004	0	13.8	5 18e+10	8.32e+10	1.95e+01	2.20e+01	1.17e+14	4.70e+11	6.98e+10	1.31e+11	2.52e+01	2.92e+01	8.06e-01	8.93e-01
92099002	1.5	17.6	1.07e+11	1.21e+11	2.87e+01	3.62e+01	1.00e+03	1.11e+03	1.27e+11	1.32e+11	2.82e+01	3.85e+01	2.03e+00	1.86e+00
92100003	2.4	43.5	1.79e+12	2.63e+12	4.06e+01	8 11e+01	7 39e+02	1.35e+03	1.38e+12	3.57e+12	4.56e+01	1.23e+02	2.08e+00	1.46e+00
92100014	1 6	20.1	3.77e+11	2.90e+11	5.77e+01	5 47e+01	5.81e+02	8.43e+02	2.83e+11	2.20e+11	5.50e+01	6.69e+01	2.42e+00	2.20e+00
92101008	0	7.9	1.38e+10	1.30e+10	1.89e+01	8.64e+00	6.05e+11	3 43e+02	1.54e+10	1.30e+10	1.65e+01	1.53e+01	1.73e+00	2.24e+00
92102027	0	9.2	1.85e+09	1.79e+09	8.87e+00	5 13e+00	1 47e+03	3.59e+02	1.32e+09	1.50e+09	7.82e+00	1.95e+01	3.03e+00	1.46e+00
92104021	1.3	27.3	7.81e+10	3.23e+10	2.26e+01	5.20e+00	2.33e+03	9.82e+02	1.08e+11	3.17e+10	1.89e+01	5.49e+00	1.36e+00	2.03e+00
92105003	1.5	31.6	1.44e+11	2.70e+11	4.45e+01	2.99e+01	1.85e+03	1.30e+03	1.70e+11	3.74e+11	4.82e+01	9 74e+01	1.47e+00	1.30e+00
92106023	0	9 1	2.69e+10	1.95e+10	2.09e+01	1.91e+01	1.07e+03	5.26e+02	2.30e+10	1.53e+10	1.99e+01	2.04e+01	2 12e+00	2.47e+00
92107001	0	7.5	2.98e+10	3.11e+10	1.95e+01	2.03e+01	5.09e+02	6.69e+02	2.57e+10	2.34e+10	1.89e+01	2.03e+01	2 81e+00	2.28e+00
92108002	2.5	70.4	5.44e+11	2.27e+12	6.98e+01	7.34e+01	1 61e+03	1.36e+03	6 89e+11	3.12e+12	7.08e+01	1.00e+02	1.28e+00	1.33e+00
92108006	1.7	14.7	4.36e+11	1.54e+11	2.37e+01	2.54e+01	6.85e+02	2.05e+03	3.77e+11	1.32e+11	2.29e+01	2.32e+01	2.48e+00	1.71e+00
92108010	0	9.4	5 55e+10	2.74e+10	1.31e+01	2.11e+01	3.79e+02	2.46e+03	4.78e+10	2.88e+10	1.73e+01	1 98e+01	2.43e+00	1 69e+00
92108011	2.3	30.7	7.03e+11	5.20e+11	6.29e+01	5 07e+01	1.47e+03	2.17e+03	8 63e+11	5.21e+12	8.02e+01	3.79e+02	1.58e+00	1.05e+00
92109017	1.8	21.7	5.74e+11	1.93e+11	5.69e+01	3.18e+01	9.43e+02	1.06e+03	5.27e+11	1.79e+11	6.31e+01	3.65e+01	1.85e+00	1.94e+00
92110016	2.8	48.5	3.05e+14	4.35e+12	1 17e+02	9 07e+01	6.78e+02	1.26e+03	3.44e+12	7.20e+12	8.15e+01	1.38e+02	2.55e+00	1.56e+00
92111007	1 6	35.0	2.75e+11	1.45e+11	4.26e+01	2.47e+01	9.63e+02	1.07e+03	2.90e+11	1.63e+11	4.98e+01	2.63e+01	1.88e+00	1.88e+00
92112004	0	9.1	5.52e+09	2.66e+09	2.78e+01	2.37e+01	3.03e+12	1.28e+03	5.25e+09	2.71e+09	5.44e+01	2.94e+01	1.09e+00	1.70e+00
92113004	2.8	15.0	2.76e+12	4.69e+12	3.87e+01	6 30e+01	5.53e+12	1.67e+04	6.77e+12	9.91e+12	2.71e+02	1.37e+02	8.18e-01	1.23e+00
92113018	0	14.6	3.27e+10	3.45e+10	2.14e+01	1.56e+01	4.77e+02	8.89e+02	2.69e+10	2.56e+10	2.44e+01	1.45e+01	2.50e+00	2.42e+00
92114002	4.6	114.6	4.18e+15	7.56e+14	6.04e+02	3 29e+01	9 77e+02	1.06e+03	8.87e+15	3.02e+15	6.53e+02	1.43e+03	1.99e+00	1.26e+00
92114013	3.6	107.5	4.05e+13	3.44e+13	1.62e+02	1.23e+02	1.12e+03	1.28e+03	4.20e+13	3 80e+13	1.66e+02	1.40e+02	1.95e+00	1.59e+00
92114016	0	108.6	2.64e+14	3.49e+13	2.23e+02	5.15e+01	1.23e+03	1.02e+03	3.28e+14	4.67e+13	2.90e+02	1.33e+02	1.69e+00	1.47e+00
92114074	3.8	112.5	3.53e+14	3.35e+13	2.81e+02	9.88e+01	1.23e+03	1.23e+03	4.73e+14	1.42e+14	3.38e+02	1.92e+02	1.75e+00	1.13e+00
92114179	3.7	106.5	2.66e+14	3.37e+13	1.53e+02	8.64e+01	6.44e+02	9.53e+02	9.45e+13	3.66e+13	1.15e+02	7.38e+01	3.02e+00	2.31e+00
92114359	3.1	111.9	1.56e+15	1.74e+14	3.32e+02	2.15e+02	9.46e+02	9.81e+02	1.42e+15	1.78e+14	3.13e+02	2.08e+02	2.10e+00	2.08e+00
92120050	2.7	42.0	2.49e+12	4.78e+12	4 47e+01	7.29e+01	6 52e+02	1.15e+03	1.81e+12	5.29e+12	4.65e+01	8.12e+01	2.63e+00	1.75e+00
92131029	0	11.7	4.54e+10	1.65e+10	1.61e+01	1 62e+01	3.82e+02	8.61e+02	3.43e+10	1.44e+10	1.89e+01	1 69e+01	2.96e+00	2.07e+00
92131048	0	31.7	6.22e+10	1.84e+15	1.97e+01	2.01e+01	7.61e+02	8.46e+02	5.77e+10	1.56e+11	2.23e+01	2.22e+01	2 30e+00	2.23e+00
92134017	1.7	10.2	2.54e+11	2.33e+11	2.53e+01	1.43e+01	4.55e+03	6.08e+02	3.36e+11	2.04e+11	3.04e+01	1.48e+01	1.39e+00	2.57e+00
92134019	1.8	13.7	3.95e+11	2.35e+11	1.84e+01	2.28e+01	3.36e+02	6.72e+02	2.61e+11	1.72e+11	2.16e+01	1.93e+01	3.46e+00	2.85e+00
92134025	1.5	13.6	3.14e+11	1.45e+11	1.88e+01	1.43e+01	2.81e+02	4.00e+02	1.79e+11	9.17e+10	2.17e+01	1 67e+01	3.77e+00	3.46e+00
92139022	1.3	11.5	1.22e+11	1.14e+11	5.33e+01	6.21e+01	1.58e+04	9.94e+02	1.35e+11	1.16e+11	6.16e+01	6 31e+01	1.59e+00	1.99e+00
92140014	0	13.6	2.56e+10	5.59e+10	-	2.55e+01	-	1.11e+05	4.14e+10	7.15e+10	3.77e+01	2 99e+01	4.11e-01	1.08e+00
92141012	0	10.4	1.23e+10	1.96e+10	6.21e-03	1.43e+01	2.50e+03	1.65e+03	2.05e+10	1.99e+10	1.28e+01	1 29e+01	3.09e-08	1.78e+00
92141020	2.7	34.0	2.59e+12	1.88e+12	6.37e+01	7.85e+01	3.63e+02	8.51e+02	1.49e+12	1.66e+12	6.60e+01	6 38e+01	3.14e+00	2.37e+00
92142001	0	30.4	1.37e+11	1.49e+11	2.84e+01	4.28e+01	4.32e+02	1.16e+03	8.53e+10	1.49e+11	3.28e+01	4 38e+01	3.24e+00	1.80e+00
92145002	0	12.5	1.21e+10	1.09e+10	1.76e+01	1 65e+01	4.07e+10	2.16e+03	1.59e+10	1.12e+10	1.92e+01	1.30e+01	9.03e-01	2.16e+00
92147012	2.0	13.0	5.60e+11	5.53e+11	1.48e+01	1.88e+01	3.04e+02	7.44e+02	4.91e+11	4.75e+11	3.75e+01	2.41e+01	1.65e+00	1 90e+00
92150002	1.8	13.0	8.34e+11	3.40e+11	2.14e+01	2.51e+01	2.40e+02	4.18e+02	3.72e+11	2.31e+11	2.40e+01	2.89e+01	3.89e+00	3.13e+00
92151010	2.0	32.1	7.39e+11	8.24e+11	3.34e+01	2.43e+01	8.20e+02	8.14e+02	6.48e+11	6.43e+11	3.36e+01	2.38e+01	2 27e+00	2.52e+00
92151018	0	14.3	3.41e+10	5.49e+10	1.64e+01	2.27e+01	1.47e+11	1.31e+04	4.13e+10	5.58e+10	1.11e+01	2.17e+01	1.46e+00	1.15e+00
92155025	2.3	34.3	6.42e+11	1.01e+12	6.09e+01	5.09e+01	1.42e+03	1.14e+03	7.02e+11	1.22e+12	6.40e+01	5.51e+01	1.74e+00	1.77e+00
92156003	0	9.2	9.41e+09	2.54e+09	8.55e+00	1.03e+01	6.17e+02	2.52e+03	-	2.87e+09	-	7.70e+00	-	2.63e+00

Table 1a. (continued)

Event	M_L	D, km	Model 1 (n=2, Q=?)						Model 2 (n=?, Q_P=Q_S=1000)					
			M_0P, N m	M_0S, N m	rP, m	rS, m	Q_P	Q_S	M_0P, N m	M_0S, N m	rP, m	rS, m	nP	nS
92157018	0	9.4	2.63e+09	8.04e+08	4.54e+00	1.04e+01	7.67e+02	1.00e+13	4.60e+09	2.65e+09	-	-	-	-
92161010	2.5	38.8	2.29e+12	1.81e+12	4.01e+01	3.99e+01	6.40e+02	1.03e+03	1.75e+12	1.84e+12	3.81e+01	4.01e+01	2.86e+00	1.93e+00
92162011	0	9.4	5.53e+09	4.10e+09	2.12e+01	1.61e+01	2.62e+12	2.04e+03	8.17e+09	3.69e+09	4.60e+01	1.44e+01	8.75e-01	1.77e+00
92165009	2.3	30.7	1.37e+12	1.21e+12	4.47e+01	3.78e+01	7.36e+02	1.05e+03	9.51e+11	1.07e+12	4.35e+01	3.76e+01	2.39e+00	1.95e+00
92167014	0	9.9	3.91e+10	6.21e+10	1.94e+01	3.00e+01	2.40e+11	2.44e+04	6.79e+10	9.51e+10	2.66e+01	4.61e+01	7.97e-01	1.22e+00
92167016	0	7.5	2.06e+10	1.18e+10	1.23e+01	1.86e+01	1.90e+02	3.75e+02	1.34e+10	8.47e+09	2.84e+01	1.92e+01	1.94e+00	2.87e+00
92169023	1.3	15.7	1.16e+11	1.21e+11	2.31e+01	4.48e+01	3.65e+02	7.67e+02	7.33e+10	1.04e+11	2.45e+01	3.26e+01	3.54e+00	2.37e+00
92171015	0	15.2	3.21e+10	5.29e+10	1.86e+01	2.45e+01	1.30e+03	1.28e+03	3.25e+10	4.86e+10	1.60e+01	2.52e+01	2.24e+00	1.76e+00
92172016	1.4	13.7	1.82e+11	1.15e+11	2.11e+01	1.50e+01	4.06e+02	4.81e+02	1.32e+11	7.43e+10	2.48e+01	1.65e+01	2.54e+00	3.11e+00
92173009	0	14.6	3.58e+10	3.61e+10	1.95e+01	1.46e+01	1.98e+11	2.16e+03	4.88e+10	3.76e+10	1.19e+01	1.16e+01	9.74e-01	1.57e+00
92173018	2.5	9.4	3.36e+12	-	3.56e+01	-	3.35e+02	-	2.34e+12	2.12e+12	3.69e+01	3.29e+01	2.64e+00	2.55e+00
92173019	0	9.3	1.89e+10	1.48e+10	1.79e+01	1.81e+01	2.20e+13	2.75e+03	2.40e+10	1.71e+10	2.29e+01	1.74e+01	9.71e-01	1.58e+00
92173020	1.9	9.3	5.91e+11	4.99e+11	3.90e+01	2.36e+01	1.10e+12	6.16e+02	6.24e+11	4.33e+11	3.47e+01	2.29e+01	1.83e+00	2.43e+00
92173021	0	9.3	4.46e+10	3.22e+10	2.35e+01	2.04e+01	5.45e+03	2.02e+03	5.57e+10	3.33e+10	2.44e+01	2.30e+01	1.40e+00	1.54e+00
92174003	1.3	9.4	1.94e+11	9.43e+10	2.29e+01	2.03e+01	8.50e+02	1.11e+03	1.54e+11	9.43e+10	2.33e+01	1.98e+01	2.05e+00	1.98e+00
92175012	0	9.8	-	1.79e+10	-	9.98e+00	-	7.99e+02	1.96e+10	1.59e+10	1.21e+01	9.44e+00	2.42e+00	3.09e+00
92180005	2.3	39.9	2.00e+12	2.85e+12	9.26e+01	5.33e+01	1.09e+03	1.05e+03	2.31e+12	2.83e+12	1.10e+02	4.23e+01	1.82e+00	2.08e+00
92180010	3.6	95.9	2.10e+13	2.51e+13	1.13e+02	1.06e+02	6.22e+02	8.05e+02	5.12e+13	2.49e+13	1.38e+02	8.82e+01	2.56e+00	2.57e+00
92250045	1.5	18.7	1.00e+11	8.96e+10	3.07e+01	3.04e+01	2.20e+03	1.84e+03	1.13e+11	1.01e+11	3.20e+01	3.41e+01	1.53e+00	1.44e+00
92251043	0	19.2	2.47e+10	3.10e+10	3.30e+01	2.85e+01	2.31e+10	1.84e+03	2.86e+10	3.85e+10	-	3.07e+01	-	1.38e+00
92253019	0	10.2	3.04e+10	1.76e+10	1.52e+01	1.96e+01	4.36e+02	5.97e+02	2.57e+10	1.48e+10	2.02e+01	1.82e+01	2.17e+00	2.51e+00
92253026	0	20.5	5.49e+10	3.47e+10	1.58e+01	1.93e+01	6.43e+02	9.55e+02	4.64e+10	3.61e+10	1.75e+01	1.79e+01	2.72e+00	2.24e+00
92255034	0	12.5	4.74e+11	1.23e+11	5.27e+01	2.74e+01	6.09e+02	4.31e+02	4.12e+11	8.89e+10	4.94e+01	2.85e+01	2.32e+00	2.89e+00
92256053	0	8.7	4.19e+10	2.99e+10	3.37e+01	2.79e+01	7.27e+13	9.97e+02	4.60e+10	2.85e+10	5.29e+01	2.68e+01	1.25e+00	2.06e+00
92261027	2.2	12.1	1.40e+12	1.13e+12	4.60e+01	6.96e+01	4.35e+02	8.02e+02	9.34e+11	1.12e+12	4.69e+01	6.01e+01	2.42e+00	2.22e+00
92263006	1.2	12.1	1.17e+11	1.11e+11	5.56e+01	5.59e+01	1.71e+03	1.04e+03	1.43e+11	1.08e+11	5.61e+01	3.63e+01	1.85e+00	2.14e+00
92264030	0	12.6	6.38e+09	8.76e+09	1.26e+01	2.11e+01	2.79e+03	1.04e+04	8.21e+09	4.94e+10	1.07e+01	1.99e+01	2.45e+00	1.26e+00
92265030	2.4	36.9	3.65e+10	3.22e+10	1.31e+01	1.15e+01	1.53e+03	1.85e+03	-	-	-	-	-	-
92267031	1.8	21.6	1.98e+11	8.86e+10	2.89e+01	2.41e+01	7.88e+02	1.35e+03	1.98e+11	9.22e+10	2.96e+01	2.39e+01	2.06e+00	1.64e+00
92269045	0	12.1	1.41e+10	1.71e+10	1.73e+01	1.21e+01	3.00e+02	4.35e+02	1.08e+10	1.07e+10	2.64e+01	1.55e+01	2.35e+00	2.96e+00
92273006	0	10.7	5.05e+10	4.16e+10	1.90e+01	1.60e+01	5.81e+02	9.25e+02	4.64e+10	4.35e+10	2.15e+01	1.91e+01	2.18e+00	1.86e+00
92276027	1.8	21.9	4.29e+11	3.52e+11	2.06e+01	1.82e+01	4.62e+02	7.19e+02	2.93e+11	2.46e+11	2.26e+01	1.85e+01	3.23e+00	2.65e+00
92277028	0	5.0	1.35e+10	5.58e+09	1.47e+01	1.16e+01	4.31e+02	6.48e+02	1.17e+10	5.25e+09	1.52e+01	1.13e+01	2.70e+00	2.68e+00
92278016	1.2	16.7	1.36e+11	6.04e+10	4.39e+01	3.13e+01	5.57e+02	7.24e+02	1.15e+11	5.22e+10	4.38e+01	2.87e+01	2.43e+00	2.49e+00
92278031	2.0	25.1	2.92e+11	4.40e+11	2.35e+01	3.18e+01	7.80e+02	1.11e+03	2.60e+11	4.54e+11	2.33e+01	3.20e+01	2.43e+00	1.89e+00
92279046	0	13.2	2.41e+10	2.76e+10	1.28e+01	1.53e+01	3.20e+02	6.18e+02	2.17e+10	1.81e+10	2.49e+01	1.51e+01	2.02e+00	2.94e+00
92286041	0	9.5	3.42e+10	7.79e+09	8.74e-03	1.30e+01	3.09e+02	3.65e+09	-	8.44e+09	-	9.69e+00	-	1.07e+00
92289036	0	10.9	5.70e+10	5.91e+10	2.62e+01	3.05e+01	6.68e+02	6.56e+02	4.85e+10	5.08e+10	2.46e+01	2.66e+01	2.39e+00	2.40e+00
92290022	0	14.3	1.49e+10	1.05e+10	5.17e-03	7.73e+00	4.88e+02	8.49e+02	1.96e+10	1.03e+10	2.73e+01	8.02e+00	7.62e-01	2.74e+00
92291003	0	13.8	2.06e+10	2.84e+10	1.73e+01	7.54e+00	9.50e+02	5.08e+02	2.09e+10	2.44e+10	1.61e+01	1.41e+01	2.36e+00	2.13e+00
92291004	0	13.8	3.41e+10	5.92e+10	1.58e+01	1.03e+01	1.01e+03	7.51e+02	3.52e+10	5.29e+10	1.26e+01	1.20e+01	3.68e+00	2.17e+00
92291018	1.5	15.3	1.62e+11	1.24e+11	2.18e+01	2.71e+01	6.10e+02	9.39e+02	1.36e+11	1.06e+11	2.28e+01	2.64e+01	2.48e+00	2.10e+00
92296050	1.4	16.9	8.77e+10	1.23e+11	3.11e+01	3.11e+01	1.21e+03	2.02e+03	7.66e+10	1.39e+11	3.02e+01	2.87e+01	1.93e+00	1.53e+00
92297002	2.1	37.8	1.68e+12	1.21e+12	7.40e+01	3.63e+01	8.46e+02	1.03e+03	1.83e+12	1.59e+12	8.60e+01	5.75e+01	2.03e+00	1.82e+00

Table 1a. (continued)

Event	M_L	D, km	Model 1 (n=2, Q=?)						Model 2 (n=?, Q_P=Q_S=1000)					
			M_0P, N m	M_0S, N m	rP, m	rS, m	Q_P	Q_S	M_0P, N m	M_0S, N m	rP, m	rS, m	nP	nS
92301039	0	14.9	4.57e+10	2.91e+10	3.76e-03	2.19e+01	6.70e+02	6.13e+10	-	4.94e+10	-	4.00e+01	-	7.52e-01
92302040	2.5	34.0	1.47e+12	1.02e+12	1.18e+01	4.44e+01	4.80e+02	2.43e+03	8.82e+11	9.63e+11	3.29e+01	4.31e+01	1.99e+00	1.09e+00
92303027	0	15.4	3.13e+10	2.11e+10	1.61e+01	2.28e+01	1.49e+03	3.46e+11	3.28e+10	2.36e+10	1.32e+01	2.45e+01	2.44e+00	9.65e-01
92306011	1.1	13.9	5.46e+10	6.07e+10	2.06e+01	1.73e+01	4.34e+11	2.88e+03	6.50e+10	5.95e+10	1.71e+01	1.36e+01	1.50e+00	1.91e+00
92306016	0	13.7	1.11e+10	1.45e+10	-	1.41e+01	-	2.26e+03	1.40e+10	1.49e+10	1.33e+01	1.07e+01	2.30e+00	1.73e+00
92308012	0	13.6	1.01e+10	1.92e+10	2.29e+01	7.15e+00	2.51e+12	4.12e+02	-	1.44e+10	-	1.84e+01	-	1.90e+00
92319013	3.5	84.3	4.00e+13	1.09e+13	6.17e+01	5.08e+01	8.34e+02	1.19e+03	2.48e+13	1.54e+13	6.89e+01	4.16e+01	2.25e+00	1.32e+00
92319014	3.4	85.5	3.24e+13	7.90e+12	1.05e+02	3.95e+01	1.00e+03	1.24e+03	2.96e+13	9.80e+12	1.25e+02	4.96e+01	1.72e+00	1.11e+00
92319036	0	14.5	7.07e+10	7.69e+10	1.19e+01	1.58e+01	4.74e+02	7.91e+02	6.66e+10	6.07e+10	1.57e+01	1.57e+01	2.41e+00	2.37e+00
92332050	4.1	56.6	2.65e+13	1.68e+14	5.78e+01	1.01e+02	8.48e+02	1.03e+03	2.05e+13	1.87e+14	6.36e+01	1.19e+02	2.23e+00	1.87e+00
92334042	1.5	13.2	2.22e+11	1.58e+11	3.90e+01	2.52e+01	1.08e+13	1.14e+03	2.48e+11	1.37e+11	5.35e+01	2.43e+01	1.30e+00	1.96e+00
92336028	0	13.0	1.66e+10	2.12e+10	1.31e+01	7.36e+00	2.91e+10	6.41e+02	2.09e+10	2.12e+10	8.66e+00	1.11e+01	4.46e+00	1.85e+00
92351023	0	12.6	4.75e+10	3.73e+10	2.43e+01	2.20e+01	5.44e+04	7.56e+11	5.54e+10	3.55e+10	2.21e+01	1.85e+01	1.50e+00	1.37e+00
93044004	0	16.5	4.06e+11	1.82e+11	2.09e+01	3.02e+01	4.56e+02	1.33e+03	2.87e+11	1.83e+11	2.60e+01	3.05e+01	2.73e+00	1.77e+00
93044009	1.3	10.1	6.49e+11	8.16e+11	2.89e+01	2.58e+01	2.50e+10	9.00e+03	7.16e+11	8.21e+11	2.84e+01	2.53e+01	1.56e+00	1.49e+00
93044013	0	10	7.75e+10	8.94e+10	2.05e+01	1.10e+01	4.58e+09	6.41e+02	7.85e+10	8.12e+10	1.76e+01	1.43e+01	1.67e+00	2.11e+00
93045013	2.4	11.3	3.35e+12	5.11e+12	3.85e+01	3.18e+01	2.31e+11	8.64e+02	3.56e+12	4.69e+12	3.83e+01	3.07e+01	1.62e+00	2.14e+00
93052009	0	8.7	7.50e+09	5.56e+09	1.03e+01	6.73e+00	8.03e+02	5.47e+02	7.35e+09	4.93e+09	1.15e+01	1 03e+01	1.64e+00	2.49e+00
93058010	1.8	15.3	3.31e+11	3.11e+11	5.59e+00	2.25e+01	3.90e+02	9.04e+02	3.17e+11	2.78e+11	2.28e+01	2.15e+01	1.44e+00	2 23e+00
93061015	0	13.7	4.44e+10	4.77e+10	1.83e+01	-	1.29e+03	-	4.64e+10	9.02e+10	1.60e+01	1.30e+02	2.79e+00	7.09e-01
93100002	1.5	15.2	1.76e+11	2.49e+11	1.77e+01	3.48e+01	4.13e+02	1.02e+03	1.64e+11	2.26e+11	2.13e+01	3.83e+01	2.85e+00	1.88e+00
93102007	2.3	22.2	5.40e+11	3.47e+12	7.83e+01	1.01e+02	2.55e+03	8.79e+02	7.40e+11	2.59e+12	7.66e+01	6.11e+01	1.83e+00	2.23e+00
93103003	2.0	22.3	3.02e+11	6.47e+11	5.90e+01	6.79e+01	1.84e+03	1.23e+03	2.93e+11	7.44e+11	6.88e+01	8.21e+01	1.61e+00	1.74e+00
93122009	1.7	19.5	1.85e+11	1.58e+11	4.95e+01	4.35e+01	6.82e+02	8.18e+02	1.29e+11	1.23e+11	5.35e+01	2.89e+01	2.16e+00	2.79e+00
93178006	1.1	7.8	1.25e+10	1.82e+10	1.68e+01	1.31e+01	1.98e+12	7.82e+03	1.38e+10	2.06e+10	1.37e+01	1.07e+01	1.93e+00	1.56e+00
93186005	2.0	11.0	9.79e+10	2.04e+15	1.98e+01	2.97e+01	3.04e+02	4.43e+02	7.27e+10	2.21e+11	2.26e+01	1.66e+01	3.19e+00	2.96e+00

Read 5.18e+10 as 5.18×10^{10}.

D is the hypocentral distance from the borehole, and earthquakes not recorded by the SCSN are assigned M_L= 0. The event number is composed from the year (first two digits), the Julian day (next three digits), and the number of the trigger in which it was recorded (last three digits). M_0P and M_0S are the seismic moments, rP and rS are the source radii, Q_P and Q_S are the Q values, and nP and nS are the high frequency falloff rates, all from the P and S waves respectively.

Table 1b. Source Parameter Results From Models 3 and 4

Event	Model 3 (n=2, Q=1000)				Model 4 (n=?, no Q correction)					
	M_0P, N m	M_0S, N m	rP, m	rS, m	M_0P N m	M_0S N m	rP, m	rS, m	nP	nS
92098004	5.80e+10	1.27e+11	1.24e+01	1.06e+01	6.07e+10	9.56e+10	3.20e+01	2.76e+01	1.28	1.72
92099002	1.05e+11	1.19e+11	2.87e+01	3.32e+01	9.91e+10	8.35e+10	3.01e+01	2.45e+01	2.65	3.29
92100003	2.08e+12	1.99e+12	5.16e+01	4.85e+01	9.11e+11	1.31e+12	4.18e+01	5.19e+01	3.64	3.64
92100014	3.62e+11	2.98e+11	7.33e+01	6.52e+01	2.38e+11	1.92e+11	5.30e+01	4.07e+01	3.00	3.39
92101008	1.66e+10	1.43e+10	1.53e+01	1.73e+01	1.40e+10	1.05e+10	1.96e+01	1.74e+01	1.89	2.59
92102027	1.93e+09	1.28e+09	9.18e+00	1.35e+01	-	1.15e+09	-	2.16e+01	-	1.98
92104021	9.48e+10	3.17e+10	1.48e+01	5.48e+00	6.59e+10	2.30e+10	2.57e+01	1.92e+01	2.33	2.36
92105003	1.48e+11	2.00e+11	2.79e+01	2.16e+01	1.13e+11	1.90e+11	3.41e+01	4.19e+01	2.91	3.09
92106023	2.43e+10	1.75e+10	2.19e+01	2.61e+01	2.02e+10	1.28e+10	2.22e+01	2.11e+01	2.36	3.03
92107001	2.30e+10	2.62e+10	2.24e+01	2.30e+01	2.54e+10	2.02e+10	2.11e+01	2.14e+01	2.77	2.67
92108002	6.03e+11	1.93e+12	4.49e+01	4.20e+01	3.95e+11	1.28e+12	5.28e+01	5.18e+01	3.28	4.15
92108006	3.95e+11	1.35e+11	2.75e+01	2.03e+01	3.07e+11	1.04e+11	2.46e+01	2.62e+01	3.04	2.34
92108010	5.01e+10	2.79e+10	1.90e+01	1.63e+01	4.29e+10	2.37e+10	2.10e+01	2.07e+01	2.36	2.31
92108011	5.82e+11	-	4.54e+01	-	5.77e+11	-	5.75e+01	-	2.66	-
92109017	5.94e+11	1.87e+11	5.86e+01	3.07e+01	5.94e+11	1.25e+11	4.43e+01	2.49e+01	3.14	3.70
92110016	4.18e+12	3.56e+12	1.28e+02	7.49e+01	2.47e+12	1.74e+12	7.40e+01	5.53e+01	3.71	3.89
92111007	2.79e+11	1.35e+11	4.42e+01	2.25e+01	1.97e+11	-	4.40e+01	-	3.26	-
92112004	4.86e+09	2.59e+09	2.16e+01	2.18e+01	5.09e+09	2.40e+09	4.72e+01	2.53e+01	1.42	2.35
92113004	-	-	-	-	5.27e+12	6.80e+12	1.11e+02	6.99e+01	1.28	1.99
92113018	2.86e+10	2.62e+10	2.92e+01	1.66e+01	2.22e+10	1.76e+10	2.66e+01	1.64e+01	2.90	3.32
92114002	1.09e+16	6.31e+14	5.82e+02	1.65e+02	-	-	-	-	-	-
92114013	4.98e+13	3.91e+13	1.23e+02	9.72e+01	2.63e+13	1.74e+13	1.06e+02	8.52e+01	4.10	4.14
92114016	2.13e+14	3.25e+13	1.90e+02	7.64e+01	3.47e+14	2.67e+13	3.25e+02	1.25e+02	2.55	3.12
92114074	2.64e+14	2.62e+13	2.16e+02	6.06e+01	2.34e+14	1.64e+13	1.99e+02	7.06e+01	3.01	4.58
92114179	2.90e+14	3.74e+13	2.62e+02	7.72e+01	6.28e+13	1.76e+13	1.04e+02	5.69e+01	4.68	5.63
92114359	1.73e+15	1.99e+14	3.72e+02	2.18e+02	3.11e+13	-	1.36e+02	-	3.75	-
92120050	2.73e+12	3.13e+12	7.23e+01	5.54e+01	1.17e+12	2.04e+12	3.50e+01	3.95e+01	4.76	4.23
92131029	3.64e+10	1.50e+10	2.40e+01	1.74e+01	2.95e+10	1.09e+10	2.19e+01	1.88e+01	3.02	2.72
92131048	6.00e+10	2.06e+11	2.40e+01	2.61e+01	3.85e+10	9.10e+10	2.61e+01	-	3.45	-
92134017	2.61e+11	2.16e+11	2.03e+01	1.74e+01	2.94e+11	1.43e+11	3.44e+01	1.63e+01	1.72	3.22
92134019	3.04e+11	2.02e+11	3.25e+01	2.92e+01	2.21e+11	1.32e+11	2.42e+01	2.27e+01	3.49	3.40
92134025	2.12e+11	1.11e+11	3.59e+01	2.83e+01	1.50e+11	6.65e+10	2.32e+01	1.80e+01	4.15	4.27
92139022	1.15e+11	1.05e+11	4.07e+01	4.50e+01	1.21e+11	9.75e+10	5.71e+01	4.22e+01	1.95	2.60
92140014	2.69e+10	5.84e+10	8.85e+00	1.49e+01	-	4.54e+10	-	2.70e+01	-	1.94
92141012	1.53e+10	2.00e+10	-	1.19e+01	1.26e+10	1.41e+10	1.21e+01	1.59e+01	1.02	2.37
92141020	-	1.94e+12	-	9.17e+01	1.19e+12	1.06e+12	6.37e+01	4.37e+01	3.96	4.32
92142001	1.00e+11	1.45e+11	4.08e+01	3.27e+01	6.48e+10	-	3.72e+01	-	3.67	-
92145002	1.43e+10	1.11e+10	1.11e+01	1.21e+01	1.39e+10	8.19e+09	2.45e+01	1.75e+01	1.40	2.36
92147012	4.38e+11	5.13e+11	3.11e+01	2.15e+01	4.37e+11	-	4.12e+01	-	1.92	-
92150002	6.76e+11	3.59e+11	-	-	2.12e+11	1.85e+11	2.54e+01	2.77e+01	3.94	3.97
92151010	7.26e+11	7.62e+11	4.04e+01	3.15e+01	4.76e+11	4.19e+11	3.42e+01	2.53e+01	3.49	4.37
92151018	4.20e+10	4.98e+10	9.42e+00	1.23e+01	3.34e+10	4.56e+10	1.74e+01	2.25e+01	1.82	2.08
92155025	6.02e+11	9.78e+11	4.78e+01	4.02e+01	4.98e+11	6.94e+11	5.22e+01	3.75e+01	2.92	3.74
92156003	9.61e+09	2.94e+09	1.11e+01	7.98e+00	8.94e+09	2.28e+09	1.71e+01	1.11e+01	1.45	2.31
92157018	2.34e+09	1.16e+09	6.79e+00	5.41e+00	-	1.19e+09	-	2.15e+01	-	1.11
92161010	2.04e+12	1.75e+12	6.19e+01	3.72e+01	1.07e+12	1.13e+12	3.37e+01	3.47e+01	4.74	4.18
92162011	5.78e+09	3.26e+09	1.42e+01	1.32e+01	8.54e+09	2.73e+09	3.95e+01	1.72e+01	1.26	2.24
92165009	1.23e+12	1.07e+12	5.87e+01	3.41e+01	8.09e+11	7.55e+11	4.09e+01	3.10e+01	3.52	3.84
92167014	3.57e+10	4.84e+10	1.39e+01	1.83e+01	6.08e+10	7.10e+10	4.23e+01	3.84e+01	1.08	1.77
92167016	1.53e+10	1.21e+10	2.74e+01	3.13e+01	1.21e+10	7.14e+09	2.34e+01	1.94e+01	3.23	3.38
92169023	6.34e+10	1.37e+11	3.64e+01	4.31e+01	5.88e+10	9.44e+10	2.68e+01	3.61e+01	3.57	3.22
92171015	3.34e+10	4.84e+10	1.70e+01	2.01e+01	2.61e+10	3.63e+10	1.96e+01	2.54e+01	2.64	2.67
92172016	1.45e+11	8.48e+10	3.18e+01	2.49e+01	1.11e+11	6.02e+10	2.71e+01	1.78e+01	2.97	3.96
92173009	4.08e+10	3.72e+10	1.07e+01	1.10e+01	5.31e+10	2.08e+10	3.52e+01	1.63e+01	1.22	2.38
92173018	2.73e+12	2.98e+12	5.27e+01	5.37e+01	2.15e+12	1.81e+12	3.74e+01	3.13e+01	2.94	3.13
92173019	2.28e+10	1.63e+10	1.33e+01	1.38e+01	2.15e+10	1.41e+10	2.64e+01	1.92e+01	1.33	2.16
92173020	5.70e+11	5.03e+11	3.00e+01	3.00e+01	5.70e+11	3.59e+11	4.51e+01	2.27e+01	1.82	3.05
92173021	5.33e+10	3.19e+10	1.83e+01	1.65e+01	5.01e+10	2.72e+10	2.76e+01	2.33e+01	1.69	2.14
92174003	1.80e+11	9.42e+10	2.38e+01	1.95e+01	1.45e+11	7.96e+10	2.53e+01	2.25e+01	2.33	2.45
92175012	2.53e+10	1.68e+10	1.37e+01	1.24e+01	1.67e+10	7.37e+09	-	1.20e+01	-	3.05
92180005	1.86e+12	2.82e+12	8.34e+01	4.61e+01	1.45e+12	2.02e+12	7.13e+01	3.76e+01	3.07	4.23
92180010	7.21e+13	3.31e+13	2.42e+02	1.47e+02	2.74e+13	1.35e+13	1.13e+02	7.27e+01	4.13	5.10
92250045	9.79e+10	9.06e+10	2.35e+01	1.81e+01	9.33e+10	6.83e+10	3.40e+01	2.88e+01	2.18	2.63
92251043	2.57e+10	3.22e+10	1.73e+01	1.71e+01	2.58e+10	2.36e+10	4.21e+01	2.73e+01	1.65	2.65
92253019	2.76e+10	1.64e+10	2.24e+01	2.33e+01	2.29e+10	1.21e+10	2.23e+01	1.89e+01	2.50	3.19

Table 1b. (continued)

Event	Model 3 (n=2, Q=1000)				Model 4 (n=?, no Q correction)					
	M_0P, N m	M_0S, N m	rP, m	rS, m	M_0P N m	M_0S N m	rP, m	rS, m	nP	nS
92253026	4.92e+10	3.38e+10	2.27e+01	2.00e+01	3.48e+10	2.24e+10	2.38e+01	1.99e+01	2.99	3.44
92255034	4.85e+11	1.26e+11	6.27e+01	4.25e+01	3.64e+11	8.08e+10	4.75e+01	2.73e+01	2.76	3.69
92256053	4.03e+10	2.95e+10	2.60e+01	2.78e+01	4.13e+10	2.43e+10	4.94e+01	2.60e+01	1.55	2.62
92261027	1.26e+12	1.21e+12	6.16e+01	7.96e+01	8.54e+11	7.56e+11	4.72e+01	4.89e+01	2.75	2.89
92263006	1.36e+11	1.11e+11	4.86e+01	4.06e+01	1.27e+11	8.42e+10	5.24e+01	4.39e+01	2.27	2.70
92264030	8.37e+09	7.54e+09	1.11e+01	1.26e+01	6.51e+09	7.39e+09	1.44e+01	2.23e+01	2.42	2.00
92265030	4.45e+10	5.33e+10	8.38e+00	-	2.23e+10	2.25e+10	1.75e+01	1.41e+01	3.01	3.53
92267031	2.15e+11	8.55e+10	3.26e+01	1.89e+01	1.54e+11	6.38e+10	3.15e+01	2.46e+01	2.83	2.98
92269045	1.14e+10	1.23e+10	3.00e+01	1.94e+01	9.49e+09	8.16e+09	2.94e+01	1.78e+01	2.56	3.39
92273006	4.80e+10	4.05e+10	2.31e+01	1.69e+01	4.01e+10	3.54e+10	2.37e+01	2.05e+01	2.52	2.54
92276027	3.62e+11	2.86e+11	3.69e+01	2.53e+01	2.16e+11	1.52e+11	2.39e+01	1.99e+01	3.98	4.10
92277028	1.25e+10	5.51e+09	1.70e+01	1.29e+01	1.08e+10	4.65e+09	1.64e+01	1.26e+01	2.67	2.68
92278016	1.68e+11	5.95e+10	6.16e+01	3.70e+01	9.61e+10	4.07e+10	4.56e+01	3.43e+01	2.85	3.31
92278031	2.91e+11	4.75e+11	2.74e+01	3.22e+01	1.95e+11	2.97e+11	2.72e+01	3.54e+01	3.23	3.15
92279046	1.93e+10	1.96e+10	2.25e+01	2.07e+01	1.91e+10	1.33e+10	2.80e+01	1.69e+01	2.35	3.59
92286041	2.46e+10	8.31e+09	1.56e+01	9.10e+00	-	6.79e+09	-	1.54e+01	-	1.61
92289036	5.31e+10	6.84e+10	2.93e+01	3.60e+01	4.25e+10	4.10e+10	2.61e+01	2.84e+01	2.77	3.01
92290022	1.46e+10	1.06e+10	1.27e+01	8.82e+00	1.56e+10	7.35e+09	2.93e+01	1.44e+01	1.34	2.37
92291003	2.15e+10	2.51e+10	1.63e+01	1.48e+01	1.66e+10	1.82e+10	1.87e+01	1.69e+01	2.80	2.95
92291004	3.67e+10	5.46e+10	1.58e+01	1.26e+01	2.71e+10	3.95e+10	1.47e+01	1.61e+01	3.82	2.74
92291018	1.47e+11	1.14e+11	2.73e+01	2.49e+01	1.24e+11	7.84e+10	2.48e+01	2.59e+01	3.02	3.04
92296050	8.04e+10	1.15e+11	2.91e+01	1.93e+01	6.29e+10	8.98e+10	3.22e+01	2.97e+01	2.49	2.54
92297002	1.90e+12	1.36e+12	8.94e+01	4.70e+01	1.28e+12	9.13e+11	6.99e+01	4.03e+01	3.10	3.85
92301039	4.32e+10	3.72e+10	8.05e+00	9.76e+00	-	3.38e+10	-	2.85e+01	-	1.69
92302040	9.41e+11	7.83e+11	2.99e+01	2.11e+01	6.80e+11	7.64e+11	3.36e+01	3.34e+01	3.10	3.07
92303027	3.51e+10	5.17e+10	1.42e+01	1.15e+01	2.55e+10	1.85e+10	1.66e+01	2.67e+01	2.84	1.79
92306011	6.22e+10	5.98e+10	1.41e+01	1.17e+01	5.48e+10	4.58e+10	2.25e+01	1.71e+01	1.90	2.66
92306016	1.42e+10	1.50e+10	1.38e+01	9.91e+00	1.12e+10	1.08e+10	-	1.50e+01	-	2.45
92308012	1.07e+10	1.46e+10	1.49e+01	1.75e+01	1.19e+10	1.10e+10	4.00e+01	2.14e+01	1.35	2.57
92319013	4.12e+13	9.69e+12	9.32e+01	3.21e+01	1.42e+13	4.58e+12	5.80e+01	3.54e+01	4.53	5.24
92319014	3.29e+13	6.79e+12	1.05e+02	2.59e+01	1.88e+13	3.21e+12	8.03e+01	3.50e+01	3.93	5.27
92319036	6.56e+10	6.52e+10	1.73e+01	1.83e+01	5.44e+10	4.33e+10	1.89e+01	1.74e+01	2.80	3.32
92332050	4.07e+13	1.43e+14	8.13e+01	9.12e+01	1.20e+13	4.67e+13	5.34e+01	7.14e+01	3.95	4.36
92334042	2.14e+11	1.41e+11	2.71e+01	2.37e+01	2.09e+11	1.07e+11	4.71e+01	2.40e+01	1.78	2.80
92336028	2.14e+10	2.06e+10	8.09e+00	1.06e+01	1.68e+10	1.55e+10	1.34e+01	1.63e+01	1.88	2.26
92351023	5.48e+10	3.53e+10	1.76e+01	1.37e+01	5.16e+10	2.58e+10	2.51e+01	2.22e+01	1.95	1.99
93044004	3.35e+11	1.69e+11	3.31e+01	2.54e+01	2.14e+11	1.25e+11	3.01e+01	2.93e+01	2.68	2.71
93044009	6.85e+11	8.04e+11	2.37e+01	1.93e+01	7.88e+11	6.93e+11	3.19e+01	2.64e+01	1.78	2.02
93044013	8.51e+10	8.30e+10	1.57e+01	1.46e+01	7.73e+10	6.86e+10	2.04e+01	1.90e+01	2.01	2.04
93045013	3.38e+12	5.00e+12	3.07e+01	3.41e+01	3.91e+12	4.39e+12	3.98e+01	3.31e+01	1.94	2.66
93052009	7.19e+09	5.05e+09	1.12e+01	9.95e+00	6.49e+09	4.00e+09	1.57e+01	1.51e+01	1.64	1.92
93058010	3.07e+11	2.92e+11	1.73e+01	2.37e+01	2.76e+11	2.15e+11	2.70e+01	2.30e+01	1.95	3.04
93061015	4.81e+10	4.29e+10	1.73e+01	1.18e+01	3.92e+10	5.95e+10	2.03e+01	3.89e+01	2.44	1.55
93100002	1.87e+11	2.31e+11	2.71e+01	3.43e+01	1.33e+11	1.78e+11	2.42e+01	3.54e+01	3.13	2.68
93102007	8.90e+11	3.04e+12	5.50e+01	7.97e+01	5.20e+11	2.21e+12	7.81e+01	6.69e+01	2.21	3.12
93103003	3.02e+11	5.86e+11	4.32e+01	5.61e+01	2.91e+11	5.72e+11	5.69e+01	5.18e+01	2.37	2.94
93122009	1.68e+11	1.45e+11	5.72e+01	4.32e+01	1.37e+11	1.09e+11	5.06e+01	3.93e+01	2.78	3.08
93178006	1.37e+10	2.02e+10	1.35e+01	9.49e+00	1.24e+10	1.71e+10	1.67e+01	1.43e+01	2.03	1.88
93186005	8.09e+10	2.59e+11	3.05e+01	2.51e+01	6.36e+10	1.69e+11	2.44e+01	1.75e+01	3.40	3.68

See footnote to Table 1a.

Table 2. Comparison of the Mean Variance and Other Source Parameter Ratios for Each Model

Model	Variance P	Variance S	f_cP/f_cS	M_0P/M_0S	nP/nS	Q_P/Q_S
1	0.012	0.012	1.36	1.26	-	0.81
	± 0.005	± 0.004	(0.79 - 2.37)	(0.56 - 2.86)		(0.40 - 1.64)
2	0.015	0.013	1.40	1.09	0.88	-
	± 0.004	± 0.006	(0.84 - 2.34)	(0.53 - 2.21)	(0.15 - 5.24)	
3	0.005	0.018	1.25	1.25	-	-
	± 0.005	± 0.010	(0.87 - 1.80)	(0.61 - 2.56)		
4	0.014	0.015	1.24	1.33	0.84	-
	± 0.008	± 0.007	(0.90 - 1.71)	(0.68 - 2.63)	(0.67 - 1.07)	

The variance estimates are the arithmetic means of the variance/Hz of each event ±1 standard deviation. The ratios are the geometric means for all events, and the numbers in parentheses are ±1 standard deviation.

was found to be consistent with the first borehole seismograms analyzed [*Abercrombie and Leary*, 1993], and also with the present data (Table 2 and Figure 6). Seismic moments and source radii are determined for both P and S waves separately, and then the mean value is determined as the best estimate for each earthquake for each of the four models. The moments range from 10^9 to 10^{16} Nm, corresponding to M_W 0 to 4.6 [*Hanks and Kanamori*, 1979]. The relationship between moment and local magnitude determined by *Abercrombie* [1995] predicts that the smallest earthquake studied here is about M_L -1. Figure 7 shows the corner frequency values obtained for P and S waves as a function of seismic moment and M_L.

A stress drop ($\Delta\sigma$) can then be calculated from the mean estimates of seismic moment and source radius, assuming circular rupture

$$\Delta\sigma = \frac{7M_0}{16r^3} \tag{4}$$

[*Eshelby*, 1957].

Figure 8 shows seismic moment and source radius for all the earthquakes studied, comparing the results from the four models. The results of models 1, 2 and 3 are very similar with a constant stress drop. The lack of a correction for attenuation in model 4 causes the corner frequencies and stress drops of the larger more distant events to be overestimated and those of some of the smaller events to be underestimated. The advantages of earthquake recording at depth, with low attenuation and low background noise are clearly shown. Source dimensions considerably smaller than 100 m can be resolved by the relatively high frequency data. Also the resulting wide frequency bandwidth and high signal to noise ratio allow source parameters for earthquakes spanning 2 orders of magnitude in source dimension (~ 5 to 500 m) and 7 orders of magnitude in seismic moment to be determined from one instrument.

Estimation of the real errors in the source parameter measurements is difficult because of the various contributing factors. Seismic moment is independent of the actual source model used but is affected by assumptions about Q and the actual fitting errors. The moment values obtained from P and S waves are in close agreement for all the models (Table 2), but the values of moment vary between the four models by about ±50% (P waves) and slightly more for S waves. The assumption of mean radiation pattern is probably the other principal source of error in the moment estimates. Even though the borehole recordings are of the highest quality, they are still single station recordings. *Guo et al.* [1992] found that the observed radiation pattern of Loma Prieta aftershocks was not as variable as the theoretical radiation pattern for a double couple, and so single station estimates might be less in error than first thought. *Vidale* [1989] considers the effect of focal mechanism on the amplitudes recorded from the Whittier Narrows earthquake. He finds that the focal mechanism can cause a variation of about ± a factor of 2 in wave amplitude. In this study the majority of the source parameter measurements are from the mean of P and S wave estimates, and as a node in the radiation pattern of one usually corresponds to a maximum in the other, this will minimize the radiation pattern effects. The source dimension

Table 3. Comparison of the Source Parameter Values From Model 1 With Those of the Other Three Models

	M_0P	M_0S	f_cP	f_cS
Model 2/Model 1	0.92	0.92	0.90	0.94
	(0.54 - 1.55)	(0.36 - 2.40)	(0.68 - 1.21)	(0.69 - 1.28)
Model 3/Model 1	0.95	0.87	0.93	1.06
	(0.59 - 1.53)	(0.36 - 2.14)	(0.64 - 1.34)	(0.66 - 1.36)
Model 4/Model 1	0.74	0.62	0.87	0.96
	(0.42 - 1.30)	(0.38 - 2.39)	(0.62 - 1.22)	(0.66 - 1.38)

Numbers in parentheses are ±1 standard deviation.

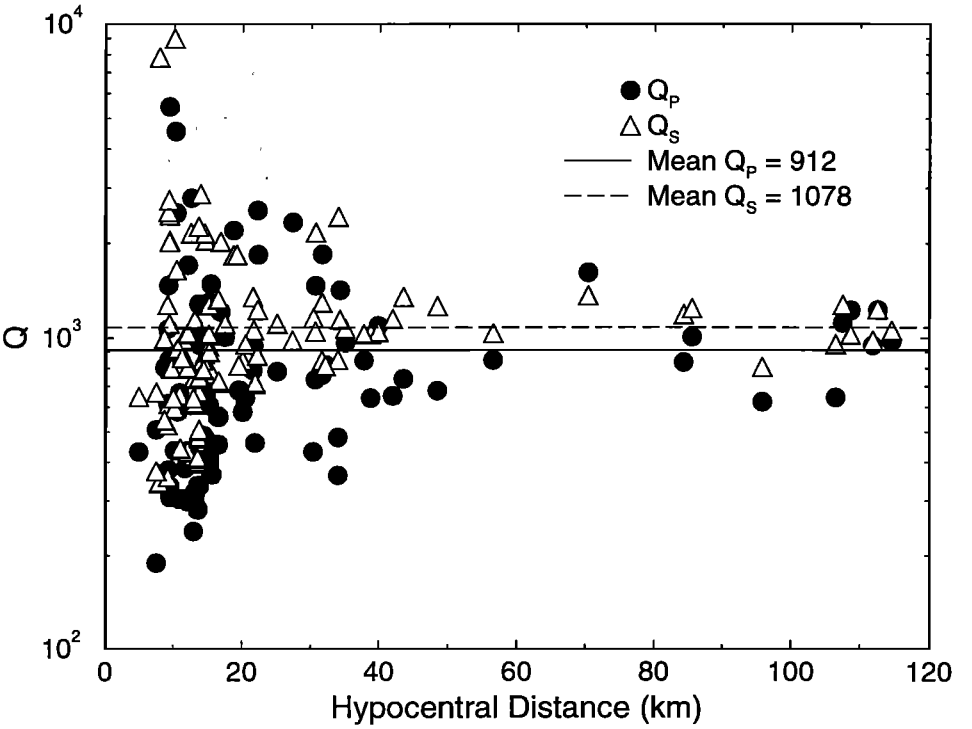

Figure 4. Compressional and shear wave Q values, plotted against distance, from fitting the earthquake spectra with model 1. The geometric mean values of Q_P and Q_S are also plotted.

estimates from the corner frequency are considerably more model dependent than the moment values. Not only does r depend on the reliability with which f_c is determined but also on the assumption of a circular source and equation (3) used to calculate r from f_c. In terms of fitting, f_c is determined about as well as Ω_0 with less than ±50% variation between the different models. The assumption of a circular source would seem reasonable for these relatively small sources, but it cannot be tested with single-station recordings. Variation of source shape and any directivity effects will result in errors when using the circular source assumption. It is unlikely, however, that all sources are in the same aspect ratio and orientation with respect to the borehole, or that all have the same rupture directivity and so although individual estimates will be affected, the average values for the whole data set are more reliable without significant bias.

To summarize, the individual earthquake estimates of moment, source dimension, and stress drop are not well constrained, although they are no worse than in many previous studies. Errors of at least a factor of 2 in moment and radius are likely, and therefore over a factor of 10 (the typical quoted error) in stress drop. In this study, however, the chief results are based on the data set as a whole and although individual estimates of moment and radius in Figure 8 are not as accurately known as would be liked, the area of moment/radius space occupied by the entire data set is considerably better constrained, and the average value of stress drop for each moment is reliable.

Radiated Seismic Energy

Recently, a number of authors have estimated radiated seismic energy from earthquakes of varying size [e.g., *Kikuchi and Fukao*, 1988, *Kanamori et al.*, 1993]. A knowledge of this parameter is clearly important to our understanding of the earthquake source

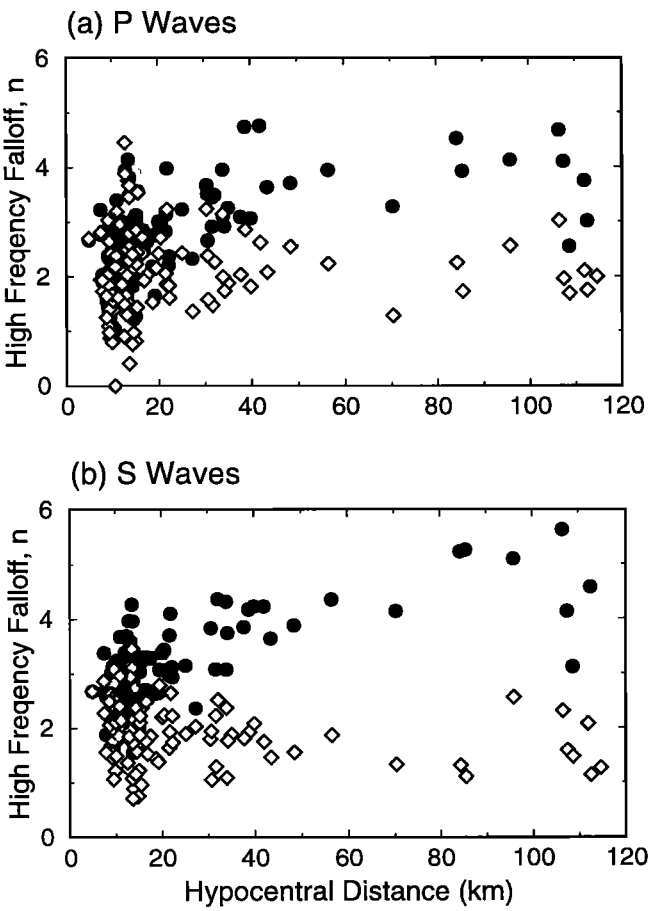

Figure 5. Comparison of P and S wave high-frequency spectral falloff (n) with distance from model 4 (no Q, solid circles) and model 2 ($Q_P = Q_S = 1000$, open diamonds). The fact that the values of n from model 2 show no dependence on distance suggests that the effect of attenuation is well corrected for.

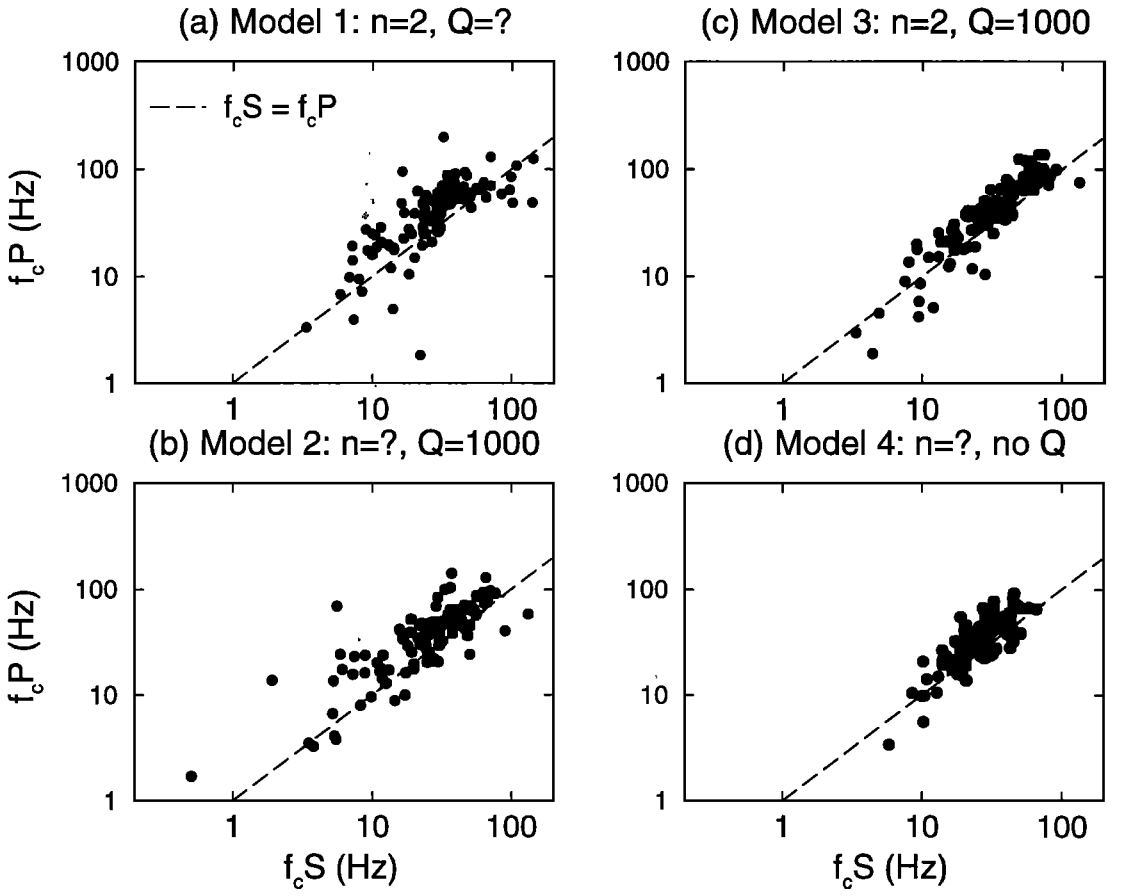

Figure 6. Comparison of the P and S wave corner frequencies from all four models. The dashed lines are those for $f_C(S) = f_C(P)$. Note that, on average, $f_C(S) < f_C(P)$ for all four models.

process. Also, estimates of apparent stress (σ_a), defined by *Wyss* [1970] as proportional to energy divided by moment, have been preferred to stress drop in some studies [e.g., *Snoke et al.*, 1983; *Houston*, 1990] on account of the large errors associated with stress drop measurement (from its dependence on corner frequency cubed). Clearly, if these small events really are similar to much larger earthquakes, then the relationship between energy and moment, as well as that between moment and source dimension, would be expected to be the same.

Seismic energy is proportional to the integral of the velocity squared seismogram over both time and frequency. For this reason it is important to consider the effects of both attenuation and the finite width of the recording system on the energy estimates. In this study therefore energy is estimated in the frequency domain, allowing more straightforward correction for attenuation and the assessment of the effect of bandwidth [*Boatwright*, 1980; *Houston*, 1990]. Following *Houston* [1990], the raw displacement spectra are converted to velocity squared and then integrated in the same frequency range that was used to fit the displacement spectra. The energy is also calculated for spectra correcting for attenuation assuming $Q_P = Q_S = 1000$ (see Figure 9). To ensure that the limited signal bandwidth is not causing significant underestimation of the energy values, the energy is only estimated for those events where the minimum signal frequency is $\leq f_C / 2$ and the maximum is $\geq 5 \times f_C$. The frequency ranges used are shown in Table 4. For the source model preferred here ($n = \gamma = 2$) then at least 80% of the radiated energy will be included in this range.

The P and S wave energy estimates (E_P and E_S respectively) are calculated by summing the integrals (I) from all three components using the formula

$$E_c = \frac{4\pi\rho c R^2 \langle U_{\phi\theta} \rangle^2}{\left(U_{\phi\theta}\right)^2} \left(I(\mathrm{Z}) + I(\mathrm{H1}) + I(\mathrm{H2})\right) \qquad (5)$$

from *Boatwright and Fletcher* [1984].

As the focal mechanisms of most events are unknown, it is assumed that $\langle U_{\phi\theta} \rangle = U_{\phi\theta}$. Missing component estimates are compensated for in the same manner as when calculating seismic moment. The S and P wave energy results are plotted in Figure 10, from spectra with and without the Q correction. The 24 earthquakes for which both E_P and E_S could be determined are then used to estimate $q = E_S/E_P$. The geometric mean, assuming negligible attenuation gives $q = 9.44$ (2.54 to 35.03) and including the Q correction gives $q = 14.31$ (4.43 to 46.26). For events for which both E_P and E_S could be determined they are summed to give the total radiated energy (E). Otherwise the missing wave energy is calculated from the available one using the empirical relationships above to obtain total energy estimates for the 32 earthquakes for which only E_P and E_S could be measured.

Estimation of the exact errors in the energy measurements is again not straightforward because of the many unknowns. In using single-station readings the effects of focal mechanism, source shape and directivity cannot be assessed. They can, however, lead to large variations in recorded energy, for example in the case of the unilateral rupture of the Landers mainshock [*Kanamori et al.*, 1992]. Other errors come from the attenuation correction, very important because of the dependence of energy on frequencies at and above the corner frequency (see Figure 9). Correcting for attenuation increases q by 50% and also increases the total energy estimates by about a factor of 4. These are therefore preferred to those without an attenuation correction.

As in the case of the source parameters moment, radius, and stress drop, however, even though the individual estimates may not be well constrained, the data set as a whole or average is much better. Attenuation and source directivity effects are unlikely to lead to a systematic bias and so will cancel out if the results are considered as an estimate of the average radiated energy for events of each moment for purposes of considering broad scaling relationships.

Discussion

High-Frequency Falloff and Attenuation

Clearly there will always be some ambiguity concerning source spectral falloff (n) and attenuation. This is true even at the high Q, downhole site because of the relatively high frequencies being considered. In model 1, $n = 2$ is assumed in order to estimate Q.

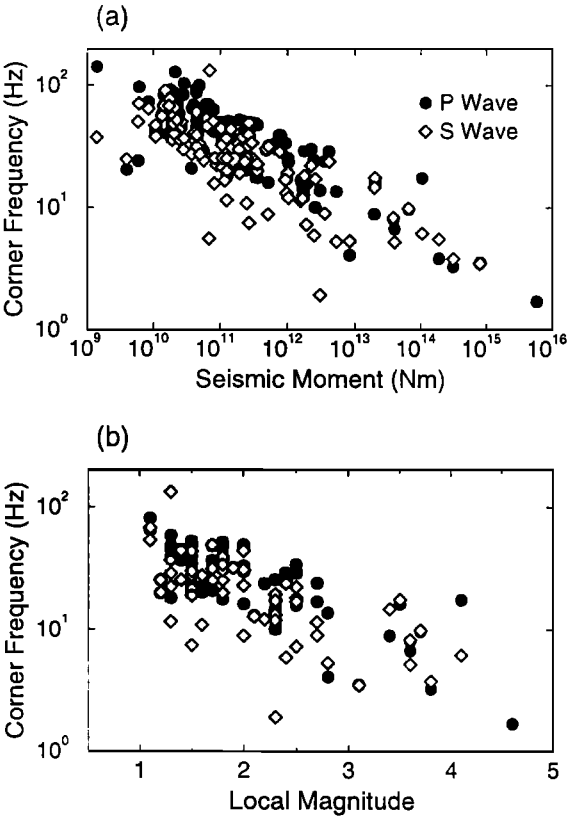

Figure 7. P and S wave corner frequencies from model 2, as a function of seismic moment and M_L

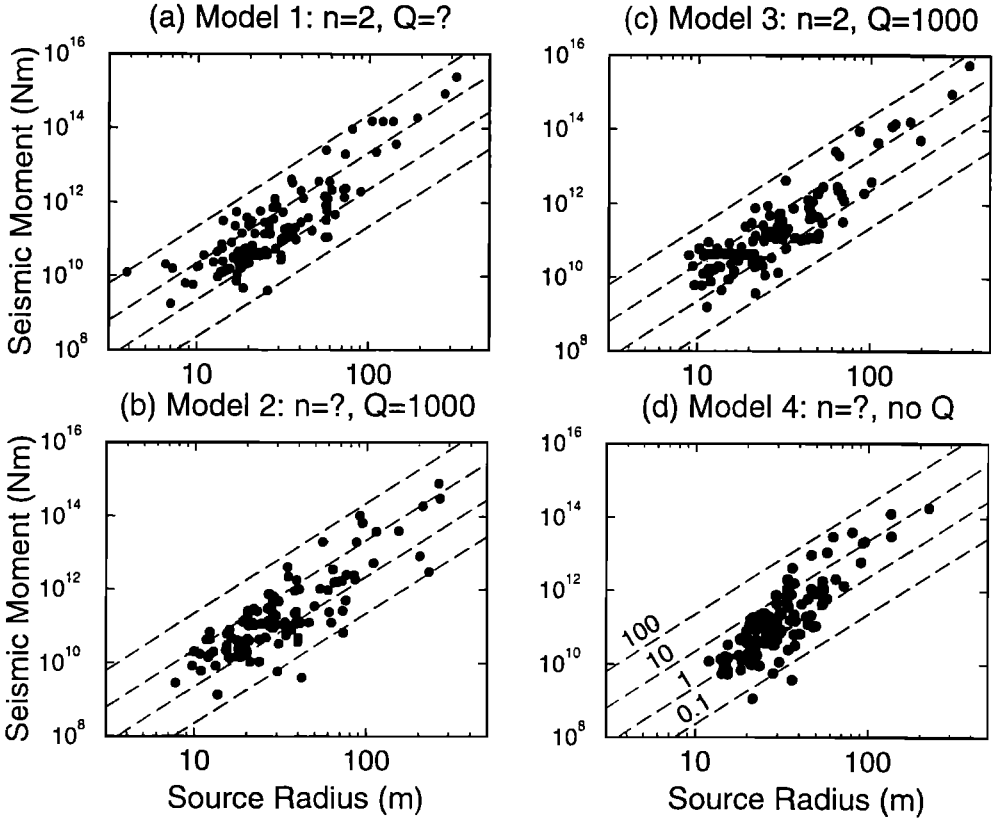

Figure 8. Seismic moment and source radius for all four models. The dashed lines of constant stress drop are calculated from equation (4) and are from 0.1 to 100 MPa.

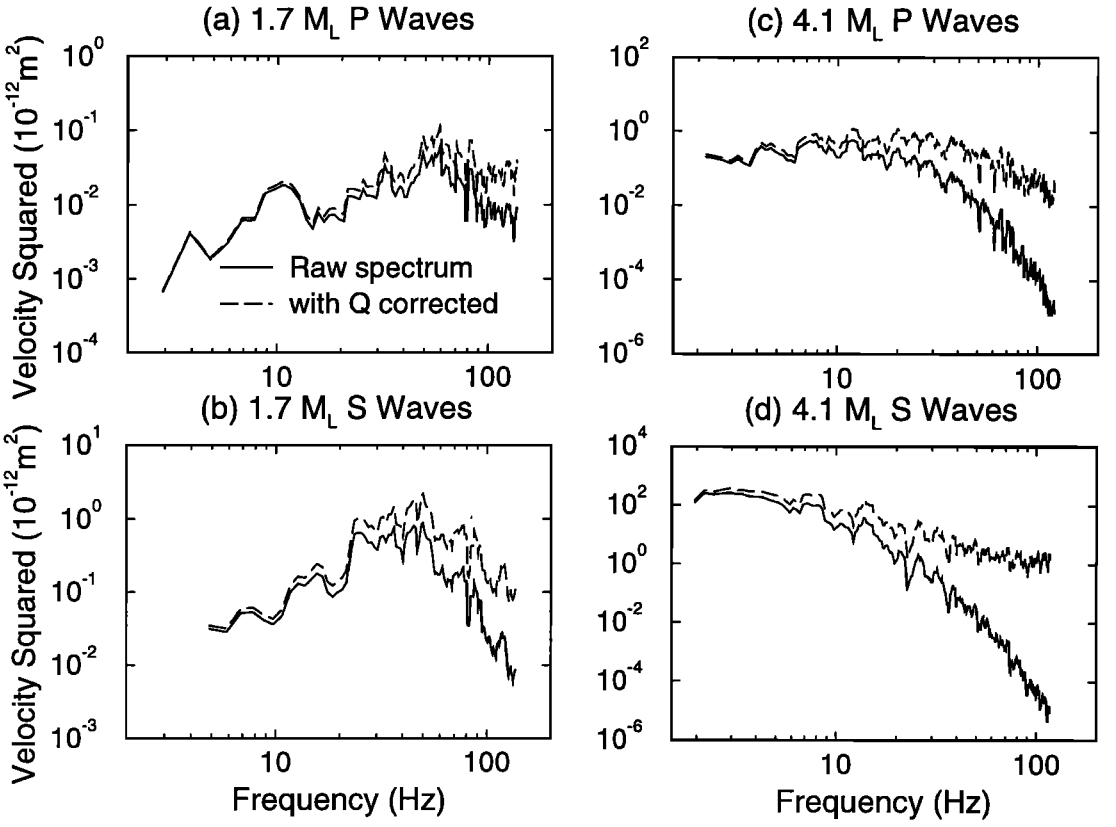

Figure 9. The seismic energy is measured by integrating the velocity squared spectra. The P and S wave spectra shown in Figure 4 are shown here with and without the correction for $Q_P = Q_S = 1000$. It is clear in Figures 9a and 9b especially how the energy is peaked around the corner frequency.

As can be seen in Figure 4, the resulting values of Q do not depend on distance, and $n = 2$ is a good average value for the closest events which are least affected by attenuation (Figure 5). $Q_P = Q_S = 1000$ and source spectral falloff $n = 2$ therefore seem good average values for the data set as a whole (models 2 and 3). In Figure 4, the principal scatter in the Q values is for the nearest events. Q is least well constrained for these earthquakes because of the small amount of attenuation they have experienced (short travel times). In Figure 5, however, we see that if Q is fixed, the same scatter in recorded spectral shape becomes a variation in source falloff. The distance dependence of n in the raw spectra (model 4) is simply an artifact of attenuation and disappears when the Q correction is applied (model 2). The large variation in Q values in Figure 4 within so small a volume has no clear explanation. It does not correlate with incoming azimuth to the borehole and so is unlikely to be caused by varying ray paths. If the scatter is interpreted as due to variation in source falloff (Figure 5, model 2), however, it could result from the variation in the take-off angles of the rays with respect to the fault plane. *Madariaga* [1976] notes that n will vary with azimuth, from about 1.5 to 2.5 in his numerical model, similar to the variation seen in Figure 5 (model 2). For these reasons, model 2 (Q fixed and n varying) is the preferred source model in this study.

The mean values of Q_P and Q_S are poorly constrained, but are both about 1000 below 2.5 km, and Q_S could be larger than Q_P. Similar values of Q have been estimated by *Hough and Anderson* [1988], also in a granite batholith. They find that Q_P is 300 to 1000 in the upper 5 km, rising to 1000 to 3000 at greater depths, and that Q_S is slightly higher than Q_P. J. D. Bott and J. C. Pechmann (Apparent decrease in stress drop with seismic moment for small earthquakes in Idaho: an artifact of attenuation, submitted to *Journal of Geophysical Research*, 1995; hereinafter referred to as submitted manuscript) invert the spectra of aftershocks to the Borah Peak earthquake to determine the attenuation structure in the area. They find that Q_S is about 241 to 1255 between 1.64 and 6.95 km, rising to around 1000 at greater depths, and that Q_P is about three times smaller.

The results of this study suggest $Q_S \geq Q_P$, as do a number of other studies such as those quoted above and that of *Modiano and Hatzfeld* [1982]. Q_P is often considered to be higher than Q_S because this is the case for anelastic attenuation in dry solids [*Knopoff*, 1964]. The Earth, however, is not simply a dry solid but contains fluids that affect the anelastic attenuation of P and S waves and its frequency dependence. Also, seismic waves are attenuated by scattering as well as anelastic (intrinsic) processes. Many studies of attenuation in the Earth's crust and mantle at a wide range of frequencies have produced a variety of results concerning the ratio and frequency dependence of Q_P and Q_S. A review of these results is not appropriate here, but the results of the present study are certainly not incompatible with our present understanding of seismic attenuation. It should also be noted that the data and methods used here are insufficient to resolve any frequency dependence of Q, or investigate the relative strengths of scattering and anelastic attenuation. For these reasons a total,

Table 4. Radiated Seismic Energy (E_P and E_S for P and S waves, respectively) Obtained From Integrating the Raw Spectra (No Q Correction) and From Integrating the Spectra After Correcting for $Q_P = Q_S = 1000$

Event	E_P, no Q, J	E_S, no Q, J	E_P, Q=1000, J	E_S, Q=1000, J	Low P, Hz	High P, Hz	Low S, Hz	High S, Hz
92098004	-	9.68e+04	-	5.58e+05	-	-	3.91	131.8
92099002	-	5.19e+04	-	1.54e+05	-	-	6.84	136.7
92100003	5.65e+04	2.17e+06	2.58e+05	1.14e+07	3.91	131.8	2.93	127.0
92100014	1.35e+04	6.01e+04	2.29e+04	1.35e+05	5.86	107.4	3.91	127.0
92105003	6 72e+03	-	3.11e+04	-	5.86	141.6	-	-
92108002	2.09e+04	1.59e+06	1.62e+05	2.01e+07	5.86	92.77	2.93	93.77
92108011	5.41e+04	-	1.75e+05	-	4.88	141.6	-	-
92109017	7.15e+04	1.55e+05	1.51e+05	6.26e+05	2.93	136.7	3.91	127.0
92110016	2.91e+05	-	6.25e+05	-	2.93	87.89	-	-
92111007	1.12e+04	-	4.57e+04	-	3.91	136.7	-	-
92112004	2.70e+01	1.15e+02	5.00e+01	2.61e+02	8.79	122.1	5.86	131.8
92113018	-	6.42e+03	-	2.47e+04	-	-	5.86	127.0
92114002	1.37e+09	-	2.22e+09	-	0.732	70.80	-	-
92114013	-	8.68e+07	-	6.97e+08	-	-	1.46	53.71
92114016	-	1.54e+08	-	1.37e+09	-	-	2.44	78.13
92114074	1.22e+07	-	3.30e+07	-	1.46	53.71	-	-
92114179	1.05e+08	2.35e+08	3.59e+08	2.54e+09	1.46	58.59	1.95	53.71
92114359	9.34e+06	4.28e+08	2.16e+07	1.53e+09	1.46	53.71	0.977	53.71
92120050	5.91e+05	7.10e+06	2.08e+06	3.29e+07	4.88	127.0	2.93	136.7
92139022	7.19e+03	2.32e+04	1.20e+04	3.84e+04	4.88	122.1	2.93	127.0
92140014	-	4.09e+04	-	1.98e+05	-	-	3.91	136.7
92141020	1.60e+05	1.60e+06	2.86e+05	3.91e+06	3.91	87.89	2.93	136.7
92142001	-	5.49e+04	-	2.73e+05	-	-	2.93	136.7
92150002	-	2.96e+05	-	6.07e+05	-	-	2.93	136.7
92161010	-	2.62e+06	-	1.27e+07	-	-	2.93	127.0
92162011	1.58e+02	-	3.44e+02	-	6.84	136.7	-	-
92165009	2.09e+05	2.53e+06	5.90e+05	1.27e+07	4.88	136.7	2.93	136.7
92167014	-	5.15e+04	-	1.50e+05	-	-	2.93	131.8
92169023	-	4.88e+04	-	9.90e+04	-	-	2.93	127.0
92180005	1.30e+05	5.91e+06	3.66e+05	2.46e+07	3.91	127.0	2.93	131.8
92180010	3.27e+06	3.12e+07	1.02e+07	1.45e+08	1.95	63.48	1.46	58.59
92250045	-	7.10e+04	-	3.42e+05	-	-	5.86	141.6
92251043	-	1.07e+04	-	5.24e+04	-	-	4.88	141.6
92255034	6.38e+04	5.36e+04	9.56e+04	1.01e+05	6.84	136.7	4.88	136.7
92256053	2.01e+03	9.75e+03	3.52e+03	1.91e+04	5.86	131.8	4.88	141.6
92261027	-	2.20e+06	-	3.53e+06	-	-	2.93	127.0
92263006	5.70e+03	3.66e+04	9.60e+03	6.44e+04	4.88	136.7	2.93	127.0
92265030	2.46e+03	-	4.22e+04	-	9.77	117.2	-	-
92278016	5.26e+03	1.22e+04	9.92e+03	3.12e+04	4.88	131.8	2.93	127.0
92278031	-	7.43e+05	-	3.53e+06	-	-	2.93	136.7
92289036	-	1.97e+04	-	3.95e+04	-	-	3.91	136.7
92296050	-	1.10e+05	-	4.22e+05	-	-	3.91	146.5
92297002	1.15e+05	1.21e+06	3.05e+05	5.06e+06	3.91	117.2	2.93	127.0
92301039	-	2.45e+04	-	1.65e+05	-	-	6.84	131.8
92302040	-	2.88e+06	-	4.18e+07	-	-	3.91	136.7
92319013	1.32e+07	5.66e+07	6.54e+07	1.44e+09	2.44	97.66	1.46	97.66
92319014	1.53e+07	2.42e+07	6.50e+07	1.21e+09	2.44	92.77	2.93	102.5
92332050	1.72e+07	8.33e+08	8.42e+07	2.35e+09	2.20	122.1	1.95	117.2
92334042	4.69e+04	-	1.06e+05	-	3.91	131.8	-	-
93044004	-	2.56e+05	-	7.95e+05	-	-	4.88	127.0
93100002	-	2.31e+05	-	5.86e+05	-	-	3.91	117.2
93102007	3.29e+04	2.84e+06	8.47e+04	5.10e+06	3.91	136.7	3.91	107.4
93103003	1.96e+04	3.94e+05	5.13e+04	1.11e+06	6.84	138.7	2.93	131.8
93122009	4.11e+03	-	8.03e+03	-	5.86	97.66	-	-

Read 5.65e+04 as 5.65×10^4.

The last four columns are the minimum and maximum frequencies over which the spectra are integrated.

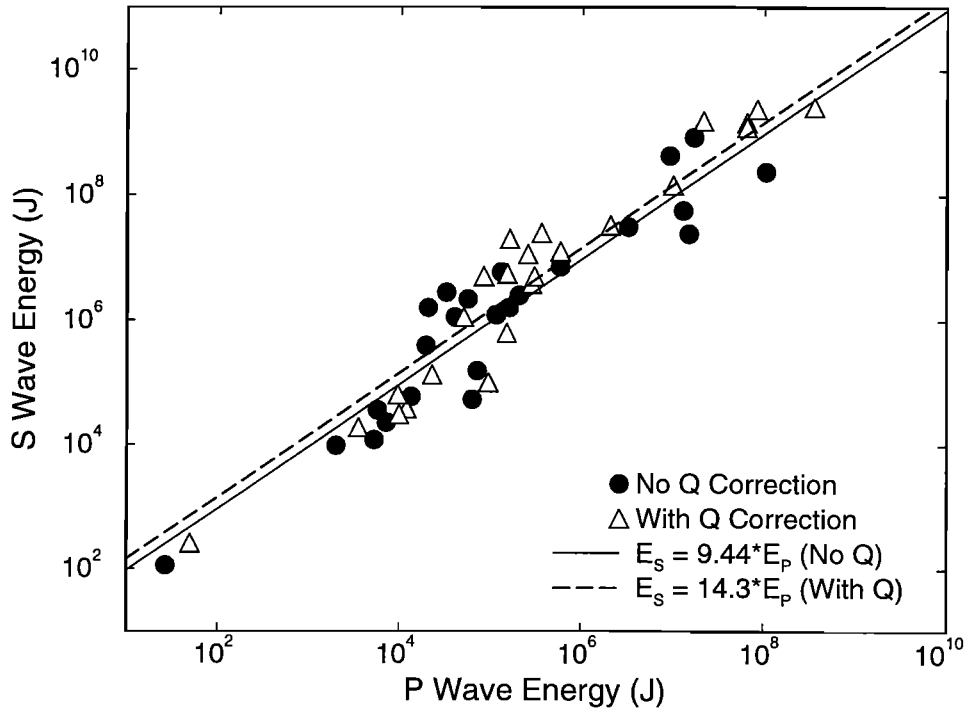

Figure 10. *S* and *P* wave energy measurements. The plotted ratios of *S* wave to *P* wave energy are the geometric means. The attenuation correction increases the ratio slightly as it affects *S* waves more than *P* waves.

frequency independent Q is assumed here and is able to model the data well.

Ratio of *P* and *S* Corner Frequencies and Radiated Seismic Energy

P wave corner frequencies determined using all four models are systematically higher than the *S* wave corner frequencies (1.40 in preferred model 2, see Table 2, Figure 6), and the ratio of $f_C(P)/f_C(S)$ is consistent with the model of *Madariaga* [1976] used to determine the source parameters. Such a shift in corner frequencies has been observed in many previous studies (see *Hanks* [1981] for a review) and could simply result from the geometric consequences of a finite source embedded in a real elastic medium ($\alpha > \beta$). There has been considerable debate, however, as to whether it is a real feature of the source or simply results from uncorrected attenuation, typically higher for *S* waves. *Molnar et al.* [1973] and *Madariaga* [1976] present source models with $f_C(P)/f_C(S) > 1$ (1.5 to 1.73), whereas *Savage* [1974] and others argue that such a shift is incompatible with Haskell-type source models and must result from attenuation. In this study, correcting for attenuation (more for *S* waves than *P* despite equal Q values because of the different travel times) actually increases the average $f_C(P)/f_C(S)$ (Table 2, Figure 6), and $f_C(P) > f_C(S)$ for all four models. It seems reasonable to conclude therefore that the corner frequency shift observed here is principally a source effect, as proposed by *Hanks* [1981]. Further analysis of individual earthquakes, without obvious source complexity and for which focal mechanisms can be determined from SCSN and the borehole data, would perhaps allow greater resolution.

The ratios of *S* wave to *P* wave energy estimated in this study (14.31 and 9.44 with and without an attenuation correction, respectively) may at first sight seem rather low. Following the model of *Boatwright* [1980], *Boatwright and Fletcher* [1984] demonstrate that

$$q = \frac{3}{2}\left(\frac{\alpha}{\beta}\right)^5\left(\frac{f_c(S)}{f_c(P)}\right)^3$$

and for Poisson's ratio of 0.25

$$q = \frac{(\sqrt{3})^7}{2}\left(\frac{f_c(S)}{f_c(P)}\right)^3 \qquad (6)$$

If the *P* and *S* corner frequencies are identical, then the ratio of *S* to *P* energy should be 23.38. The *P* and *S* wave corner frequencies of the earthquakes recorded at Cajon Pass are, however, not identical, and putting them into equation (6) predicts q=12.26 (without attenuation correction) and with the attenuation correction of Q=1000 used to calculate the energy, q = 8.52 (model 2) and 11.97 (model 3). These values are in good agreement with those estimated from the energy measurements: 9.44 (2.54 to 35.03) and 14.31 (4.43 to 46.26) without and with attenuation correction, respectively. *Bakun and McLaren* [1984] estimate q to be 4.8 for earthquakes on the creeping section of the San Andreas fault. *Boatwright and Fletcher* [1984] determine a slightly lower corner frequency shift (1.2) and correspondingly higher value of q = 16.7 for earthquakes induced by the impounding of a reservoir in South Carolina. Similar values of corner frequency shift (1.2) and q (13.9) are calculated by *Boatwright et al.* [1991] for 28 aftershocks of the Loma Prieta

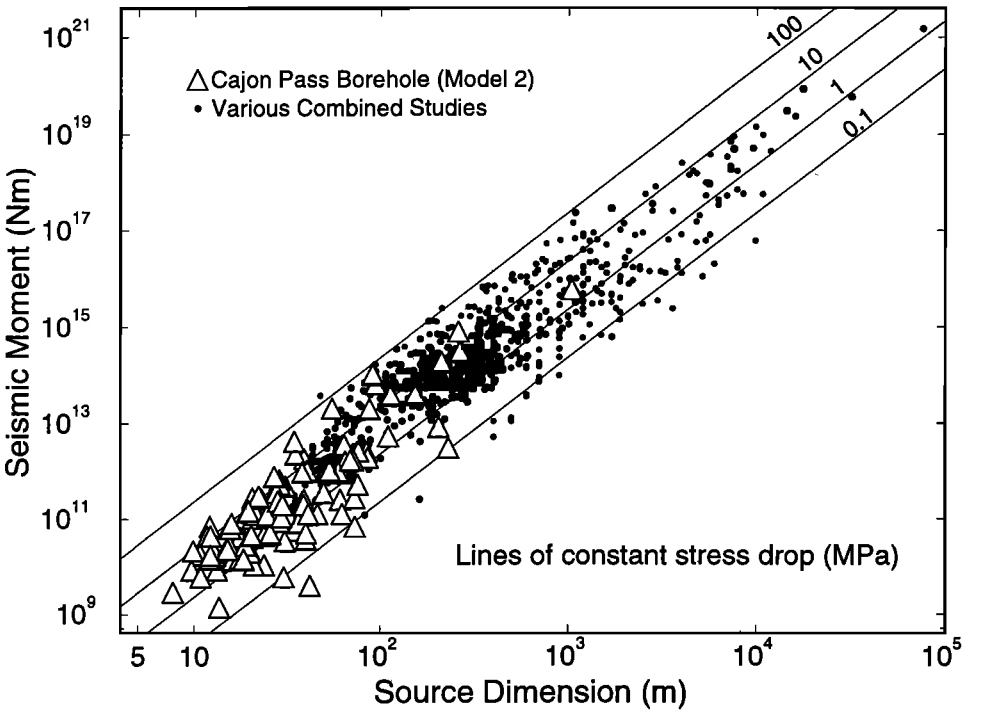

Figure 11. Seismic moment and source dimension of tectonic earthquakes. The results of this study (preferred model 2) are plotted as open triangles. The other points plotted are from the following studies, approximately in order of increasing magnitude: *Del Pezzo et al.* [1987], *Guo et al.* [1992], *Smith* [1992], *Archuleta et al.* [1982, larger events], *Mori and Frankel* [1990], *Boatwright* [1994], *Thatcher and Hanks* [1973], *Humphrey and Anderson* [1994], *Dreger and Helmberger* [1990], *Wald* [1992], and *Heaton* [1990]. Care was taken only to include studies in which a correction was made for attenuation or for which the earthquakes were large enough for attenuation effects to be ignored.

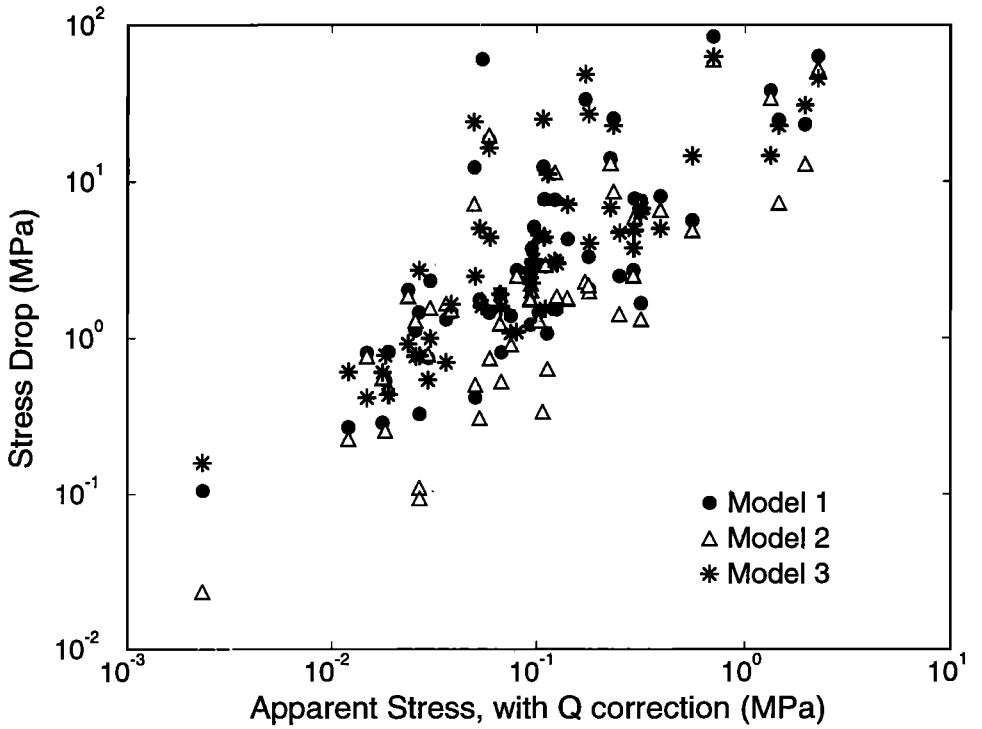

Figure 12. A comparison of the attenuation-corrected apparent stress estimates with the stress drop values obtained from the three models which also contain an attenuation correction.

earthquake. As is clear in equation (6), a small change in the corner frequency shift corresponds to a large change in q.

Seismic Moment and Source Dimension

The preferred estimates of seismic moment and source radius (model 2) for the 115 earthquakes recorded in the Cajon Pass borehole are combined with those from a number of other studies of tectonic earthquakes (Figure 11). The present study confirms the preliminary study of *Abercrombie and Leary* [1993], finding that there is no breakdown in constant stress drop scaling of earthquakes at about magnitude 3 corresponding to a dimension of about 100 m. The Cajon Pass earthquakes studied so far include events with dimensions less than 10 m. The minimum dimension of about 100 m observed by various surface studies had been postulated as a source effect [e.g., *Archuleta et al.*, 1982; *Aki*, 1987], but these results, for ordinary tectonic earthquakes on major fault zones (including the San Jacinto and San Andreas, *Abercrombie* [this issue]) show that this is incorrect, in this area at least. The "minimum dimension" observed by many surface studies should best be regarded as the limit of spatial resolution of surface data on account of the high intrinsic and scattering attenuation in the near surface rocks. *Anderson* [1986] demonstrated that reasonable values of Q would be capable of accounting for the breakdown in scaling. A number of studies have confirmed this, including that of J. D. Bott and J. C. Pechmann (submitted manuscript, 1995) who find that carefully calculated attenuation estimates are able to compensate entirely for the apparent breakdown in scaling in the aftershocks of the Borah Peak earthquake, and *Boatwright et al.* [1991] who observe no dependence of stress drop on seismic moment for 28 Loma Prieta aftershocks after correcting for attenuation. *Abercrombie and Leary* [1993] also note that tectonic earthquakes appear to have, on average, higher stress drops than induced seismic events, such as hydrofractures and mining tremors. Many small induced events have been recorded using deep instruments and the slightly lower stress drops calculated added fuel to the scaling breakdown argument. Recent work by *McGarr* [1993] has shown that the moment tensors of many mining tremors contain a significant volumetric component and that the apparent stress of those events involving significant volume reduction are significantly lower than those of pure shear sources. In this study, a very high correlation (correlation coefficient ~ 0.6, 99.9% significant; see Figure 12) is found between stress drop and apparent stress in all models. If this is also true for the induced seismic events, then it is plausible that they appear to have lower stress drops than tectonic earthquakes because of the large volumetric component in many of their sources. Either these events really involve lower stress drops, or else the application of equation 4 is incorrect in the case of volume reduction and results in an apparent lower stress drop than similar dimensioned tectonic earthquakes. It is clear therefore that in studying scaling relationships between seismic sources, we must be careful to compare only like events.

Seismic Moment and Radiated Seismic Energy

The estimates of the radiated seismic energy and seismic moment for the earthquakes recorded in the Cajon Pass borehole are combined with those determined for considerably larger

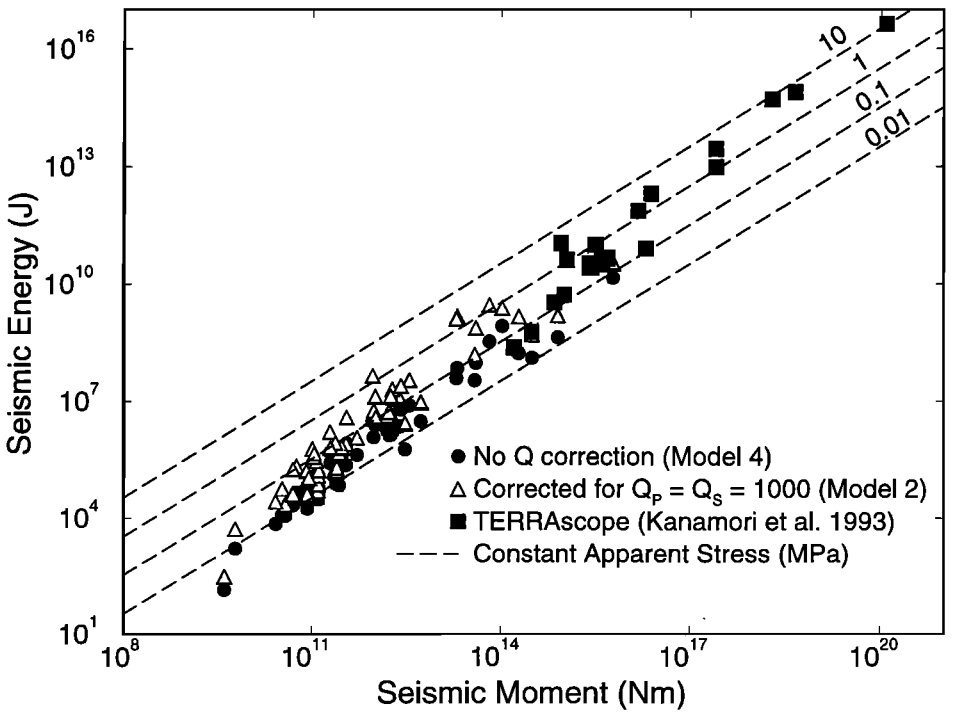

Figure 13. Seismic energy and seismic moment. The results of this study are compared with those from *Kanamori et al.* [1993] for southern California earthquakes recorded by TERRAscope. The large and small event data sets align well, but each shows an apparent underestimation of energy for the smallest events. This could result from problems with correcting for attenuation and bandwidth at the upper limit of the recording frequency range. The lines of constant apparent stress are plotted from *Wyss* [1970].

earthquakes in southern California by *Kanamori et al.* [1993] using the high dynamic range, broadband TERRAscope network in Figure 13. Both data sets are aligned but exhibit a gradual decrease in the ratio of radiated seismic energy to seismic moment in the magnitude range 7.5 to 0. These results from Cajon Pass for earthquakes smaller than about 3 M_L, however, are inconsistent with those determined by *Kanamori et al.* [1993], who find the relationship between energy and M_L, to be constant from 1 to 7 M_L. The relationship between log (M_0) and M_L, is known to change at around 3 M_L, as a result of the frequency at which M_L, is measured [*Hanks and Boore*, 1984]. Hence a straight line relationship between energy and M_L, over this range would imply a change in the relationship between energy and moment, the two more fundamental source parameters. *Kanamori et al.* [1993] apply a whole path attenuation correction but it is independent of frequency and they make no correction for finite bandwidth in their energy estimates. As the high frequency limit of TERRAscope is 7 Hz [H.-K. Thio, personal communication, 1994] they will be significantly underestimating energy for events with corner frequencies higher than this (less than about 3 M_L). A simple correction for finite bandwidth suggests that the results of *Kanamori et al.* [1993] are consistent with a similar relationship between seismic moment and seismic energy to that found here over the range of magnitudes they studied.

A number of recent studies have preferred to measure apparent stress to estimate stress drop, on account of the large errors in stress drops calculated from the corner frequency cubed (equation (4)). The fact that energy is principally released near the corner frequency and above suggests that it will be more severely affected by attenuation than just measuring the corner frequency, and apparent stress can therefore also be substantially in error for small surface recorded earthquakes.

A comparison of Figures 11 and 13 suggests that whereas $\Delta\sigma$ is constant over the whole magnitude range, σ_a gradually decreases. It is possible that this decrease in σ_a is an artifact of attenuation, but the values used here have been corrected for reasonable values of Q. Decreasing Q from 1000 to 500 would increase the energy estimates by, on average, a further factor of 3. A lower, frequency independent Q cannot be supported by the data. This increase in energy is not enough to account for the trend seen in Figure 13, even when combined with the possible 20% underestimation of energy from the finite bandwidth. A similar result of decreasing E/M_0 with seismic moment has also been observed by *Mayeda and Walter* [1994] from regional seismograms of larger events (M_w 3 - 7.3). *Abercrombie and Mori* [1994] calculated stress drop and apparent stress estimates for the Landers and Northridge earthquakes, and their larger (≥M4) aftershocks. They found that whereas stress drop is fairly constant, apparent stress decreases with moment, and that realistic attenuation corrections were unable to account for the entire trend. The two relationships found here in Figures 11 and 13 and also by *Abercrombie and Mori* [1994] are not mutually incompatible, as the stress drop is simply dependent on frequencies up to and including the first corner frequency, whereas the apparent stress (energy) is critically dependent on the shape of the spectrum at higher frequencies. For example, a gradually increasing degree of complexity of the source with increasing moment could explain the results found here. It is worth noting, however, that the values of stress drop and apparent stress calculated in this study are highly correlated (Figure 12) and neither exhibit significant dependence on seismic moment. It is therefore possible that the apparent stress may be independent of moment, and the trend seen in Figure 13 may result from an offset between the results of this study and that of *Kanamori et al.* [1993], combined with attenuation effects. For example, near-surface amplification and scattering may lead to higher estimates of radiated energy at surface sites than at borehole stations.

Conclusions

Spectral analysis of 100 earthquakes in the magnitude range -1 to 5, recorded at 2.5 km depth in granite shows the following,

1. There is no breakdown in the self similarity of the earthquake source (constant stress drop relationship) below magnitude 3. Source dimensions of less than 10 m are observed, 10 times smaller than the proposed "minimum" source dimension. The apparent breakdown in scaling and this "minimum" source dimension of about 100 m are artifacts of the severe attenuation of high frequency seismic waves in the upper kilometers of the Earth's crust.
2. The ratio of radiated seismic energy to seismic moment (apparent stress) decreases gradually with decreasing moment in the entire magnitude range (0 to 7). Whether this is due to changes in the energy radiated by the source with moment, or problems with estimating seismic energy is still unclear.
3. The ratio of S wave radiated energy to that of P waves is approximately 14 after correcting for attenuation (Q_P = Q_S = 1000). This is consistent with the observed corner frequency shift of approximately 1.25 to 1.5 obtained from fitting the displacement spectra with the same Q value.
4. Intrinsic attenuation is very low beneath 2.5 km and Q of both compressional and shear waves is about 1000.
5. The high frequency fall off $n = 2$ is a good average for the small earthquakes studied, but there is significant variation in the real fall off values.

Acknowledgments. I am grateful to P. Leary and D. Manov for installing the deep borehole seismometers; to M. Robertson, A. Martin, and L. Fields for help with the data recording, and to L. Teng, P. Davis, the California Department of Mines and Geology, and the Southern California Earthquake Center (SCEC) for generously loaning recording equipment. J. Mori, J. Vidale, J. Boatwright, A. McGarr, and the Associate Editor provided constructive reviews of the original manuscript. The borehole seismometer was installed under NSF award EAR-9004381, and R.E.A. was supported by a SCEC Visiting Fellowship and NSF award EAR-9219856. SCEC contribution 113.

References

Abercrombie, R. E., Earthquake locations using single-station deep borehole recordings: Implications for microseismicity on the San Andreas fault in southern California, *J. Geophys. Res.*, this issue.

Abercrombie, R. E., The magnitude - frequency distribution of earthquakes recorded with deep seismometers at Cajon Pass, southern California, *Tectonophysics*, in press, 1995.

Abercrombie, R. E., and J. J. Mori, Scaling of radiated energy (abstract), *E. Trans. AGU, 75 (44)*, Fall Meet. Suppl., 433, 1994.

Abercrombie, R. E., and P. Leary, Source parameters of small earthquakes recorded at 2.5 km depth, Cajon Pass, southern California: Implications for earthquake scaling, *Geophys. Res. Lett.*, *20*, 1511-1514, 1993.

Aki, K., Scaling law of seismic spectrum, *Bull. Seismol. Soc. Am.*, *72*, 1217-1231, 1967.

Aki, K., Magnitude-frequency relation for small earthquakes: A clue to the origin of f_{max} of large earthquakes, *J. Geophys. Res.*, *92*, 1349-1355, 1987.

Aki, K. and P. Richards, *Quantitative Seismology*, 932 pp., W. H. Freeman, New York, 1980.

Anderson, J. G., Implication of attenuation for studies of the earthquake source, in *Earthquake Source Mechanics*, *Geophys. Monogr.*, vol 37, edited by S. Das *et al.*, pp 311-318, AGU, Washington, D.C., 1986.

Anderson, J. G. and S. Hough, A model for the shape of the Fourier amplitude spectrum of acceleration at high frequencies, *Bull. Seismol. Soc. Am.*, *74*, 1969-1994, 1984.

Archuleta, R. J., E. Cranswick, C. Mueller, and P. Spudich, Source parameters of the 1980 Mammoth Lakes, California, earthquake sequence, *J. Geophys. Res.*, *87*, 4595-4607, 1982.

Aster, R. C., and P. M. Shearer, High-frequency borehole seismograms recorded in the San Jacinto fault zone, southern California, 2, Attenuation and site effects, *Bull. Seismol. Soc. Am.*, *81*, 1081-1100, 1991.

Bakun, W. H., and M. McLaren, Microearthquakes and the nature of the creeping-to-locked transition of the San Andreas fault zone near San Juan Bautista, California, *Bull. Seismol. Soc. Am.*, *74*, 235-254, 1984.

Blakeslee, S., and P. Malin, High-frequency site effects at two Parkfield downhole and surface stations, *Bull. Seismol. Soc. Am.*, *81*, 332-345, 1991.

Boatwright, J., A spectral theory for circular seismic sources: simple estimates of source dimension, dynamic stress drop and radiated energy, *Bull. Seismol. Soc. Am.*, *70*, 1-27, 1980.

Boatwright, J., Regional propagation characteristics and source parameters of earthquakes in northeastern North America, *Bull. Seismol. Soc. Am.*, *84*, 1-15, 1994.

Boatwright, J. and J. B. Fletcher, The partition of radiated seismic energy between *P* and *S* waves, *Bull. Seismol. Soc. Am.*, *74*, 361-376, 1984.

Boatwright, J , J. B. Fletcher and T. E. Fumal, A general inversion scheme for source site, and propagation characteristics using multiply recorded sets of moderate-sized earthquakes, *Bull. Seismol. Soc Am.*, *81*, 1754-1782, 1991.

Brune, J. N., Tectonic stress and seismic shear waves from earthquakes, *J. Geophys. Res.*, *75*, 4997-5009, 1970.

Del Pezzo, E., G. De Natale, M. Martini and A. Zollo, Source parameters of microearthquakes at Phlegraean Fields (southern Italy) volcanic area, *Phys Earth Planet. Inter. 47*, 25-42, 1987.

Dieterich, J. H., A model for the nucleation of earthquake slip, in *Earthquake Source Mechanics*, *Geophys. Monogr.*, vol 37, edited by S. Das *et al.*, pp. 37-47, AGU, Washington, D.C., 1986.

Dreger, D. S., and D. V. Helmberger, Source parameters of the Sierra Madre earthquake from regional and local body waves, *Geophys. Res. Lett.*, *17*, 1417-1420, 1990.

Eshelby, J. D., The determination of the elastic field of an ellipsoidal inclusion and related problems, *Proc. R. Soc. London A, 241*, 376-396, 1957.

Frankel, A., and L. Wennerberg, Microearthquake spectra from the Anza, California seismic network: Site response and source scaling, *Bull. Seismol. Soc. Am.*, *79*, 581-609, 1989.

Guo, H. A., A. Lerner-Lam, and S. E. Hough., Empirical Green's function study of Loma Prieta aftershocks: Evidence for fault zone complexity (abstract), *Seismol. Res. Lett.*, *63*, 76, 1992.

Hanks, T. C., Earthquake stress drops, ambient tectonic stresses and stresses that drive plate motions, *Pure. Appl. Geophys.*, *115*, 441-458, 1977.

Hanks, T. C., The corner frequency shift, earthquake source models and *Q*, *Bull. Seismol. Soc. Am.*, *71*, 597-612, 1981.

Hanks, T. C., f_{max}, *Bull. Seismol. Soc. Am.*, *72*, 1867-1879, 1982.

Hanks, T. C., and D. M. Boore, Moment-magnitude relations in theory and practice, *J. Geophys. Res.*, *89*, 6229-6235, 1984.

Hanks, T. C., and H. Kanamori, A moment magnitude scale, *J. Geophys. Res.*, *84*, 2348-2350, 1979.

Heaton, T. H., Evidence for and implications of self-healing pulses of slip in earthquake rupture, *Phys. Earth Planet. Inter.*, *64*, 1-20, 1990.

Hough, S. E., and J. G. Anderson, High frequency spectra observed at Anza, California: Implications for *Q* structure, *Bull. Seismol. Soc. Am.*, *78*, 692-707, 1988.

Houston, H., Broadband source spectrum, seismic energy , and stress drop of the 1989 Macquarie ridge earthquake, *Geophys. Res. Lett.*, *17*, 1021-1024, 1990.

Humphrey, J. R. and J. G. Anderson, Seismic source parameters from the Guerrero subduction zone, *Bull. Seismol. Soc. Am.*, *84*, 1754-1769, 1994.

Kanamori, H., H. K. Thio, D. Dreger, E. Hauksson and T. Heaton, Initial investigation of the Landers, California, earthquake of 28 June 1992 using TERRAscope, *Geophys. Res. Lett.*, *19*, 2267-2270, 1992.

Kanamori, H., J. Mori, E. Hauksson, T. H. Heaton, L. K. Hutton, and L. Jones, Determination of earthquake energy release and M_L using TERRAscope, *Bull. Seismol. Soc. Am.*, *83*, 330-346, 1993.

Kikuchi, M., and Y. Fukao, Seismic wave energy inferred from long-period body wave inversion, *Bull. Seismol. Soc. Am.*, *78*, 1707-1724, 1988.

Knopoff, L., *Q*, *Rev. Geophys.*, *2*, 625-660, 1964.

Madariaga, R., Dynamics of an expanding circular fault, *Bull. Seismol. Soc. Am.*, *66*, 639-666, 1976.

Mayeda, K., and W. R. Walter, Energy, moment and stress drop from path and site corrected regional *Lg* coda envelopes for western U.S. earthquakes (abstract), *Eos Trans. AGU, 75*(44), Fall Meet. Suppl., 482, 1994.

McGarr, A., Factors influencing the strong ground motion from mining-induced tremors, *Rockbursts and Seismicity in Mines*, edited by R. P. Young, pp. 3-12, Balkema, Rotterdam, 1993.

Modiano, T., and D. Hatzfeld, Experimental study of the spectral content for shallow earthquakes, *Bull. Seismol. Soc. Am.*, *72*, 1739-1758, 1982.

Molnar, P., B. E. Tucker, and J. N. Brune, Corner frequencies of P and S waves and models of earthquake sources, *Bull. Seismol. Soc. Am.*, *63*, 2091-2104, 1973.

Mori, J., and A. Frankel, Source parameters for aftershocks of the 1986 North Palm Springs earthquake, *Bull. Seismol. Soc. Am. 80*, 278-295, 1990.

Park, J., C. R. Lindberg and F. L. Vernon, Multitaper spectral analysis of high frequency seismograms, *J. Geophys. Res.*, *92*, 12,675-12,684, 1987.

Savage, J. C., Relation between *P*- and *S*-wave corner frequencies in the seismic spectrum, *Bull. Seismol. Soc. Am.*, *64*, 1621-1627, 1974.

Shimazaki, K., Small and large earthquakes: the effects of the thickness of seismogenic layer and the free surface, in *Earthquake Source Mechanics*, *Geophys. Monogr.* vol 37, edited by S. Das *et al.*, pp. 209-216, AGU, Washington, D.C., 1986.

Silver, L. T., and E. W. James, Geologic setting and lithologic column of the Cajon Pass deep drillhole, *Geophys. Res. Lett.*, *15*, 941-944, 1988.

Smith, K. D., Pulse width stress drops from short period records of the 1986 M_L 6.4 Chalfant, California, earthquake sequence (abstract), *Eos Trans. AGU, 73*(43), Fall Meet. Suppl., 345, 1992.

Snoke, J. A., A. T. Linde, and I. S. Sacks, Apparent stress: An estimate of stress drop, *Bull. Seismol. Soc. Am.*, *73*, 339-348, 1983.

Thatcher, W., and T. Hanks, Source parameters of southern California earthquakes, *J. Geophys. Res. 78*, 8547-8574, 1973.

Turcotte, D. L., Fractals in geology and geophysics, *Pure. Appl. Geophys.*, *131*, 171-196, 1989.

Vidale, J. E., Influence of focal mechanism on peak ground accelerations of strong motions of the Whittier Narrows, California, earthquake and an aftershock, *J. Geophys. Res.*, *94*, 9607-9613, 1989.

Wald, D. J., Rupture characteristics of California earthquakes, Ph. D. thesis, Calif. Inst. of Technol., Pasadena, 1992.

Wyss, M., Stress estimates for South American shallow and deep earthquakes, *J. Geophys. Res.*, *75*, 1529-1544, 1970.

R.E. Abercrombie, Institute of Geological and Nuclear Sciences, Kelburn Research Centre, 32 Salamanca Road, PO Box 1320, Wellington, New Zealand. (e-mail: R.Abercrombie@gns.cri.nz)

(Received April 22, 1995; revised July 25, 1995;
accepted August 2, 1995.)